Seismological Research Letters

Evaluation of the event detection level of the Cuban seismic network

--Manuscript Draft--

Manuscript Number:	SRL-D-22-00016R3
Full Title:	Evaluation of the event detection level of the Cuban seismic network
Article Type:	Article - Regular Section
Corresponding Author:	Enrico Priolo OGS Sgonico, (Trieste) ITALY
Corresponding Author Secondary Information:	
Corresponding Author's Institution:	OGS
Corresponding Author's Secondary Institution:	
First Author:	Eduardo R. Diez Zaldivar
First Author Secondary Information:	
Order of Authors:	Eduardo R. Diez Zaldivar
	Enrico Priolo
	Denis Sandron
	Viana Poveda Brossard
	Marco Cattaneo
	Simone Marzorati
	Raúl Palau Clares
Order of Authors Secondary Information:	
Manuscript Region of Origin:	CUBA
Abstract:	The detection level of a seismic network is a measure of its effective ability to record small earthquakes in a given area. It can vary in both space and time, and depends on several factors as meteorological conditions, anthropic noise, local soil conditions ¾all factors that affect the seismic noise level¾, as well as the quality and operating condition of the instruments. The ability to estimate the level of detection is of tremendous importance both in the design of a new network and in determining whether a given network can recognize seismicity consistently, or needs to be improved in some of its parts. In this paper, we determine the detection level of the Cuban seismic network using the empirically estimated seismic noise spectral level at each station site and some theoretical relationships to predict the signal amplitude of a seismic event at individual stations. The minimum local detectable magnitude thus depends on some network parameters such as the signal-to-noise ratio and the number of stations used in the calculation. We also demonstrate the effectiveness of our predictions by comparing the estimated detection level with those empirically determined from one year of data (i.e., the year 2020) of the Cuban seismic catalog. Our analysis shows, on the one hand, in which areas the current Cuban network should be improved, also depending on the regional pattern of faults, and, on the other hand, indicates the magnitude threshold that can be assumed homogeneously for the catalog of Cuban earthquakes in 2020. Since the adopted method can use current measurements of the seismic noise level (e.g., daily), the proposed analysis can also be configured for continuous monitoring of network state quality.
Suggested Reviewers:	Daniel E. McNamara mcnamara@usgs.gov

	Bladimir Moreno Toirán bladimir@cenais.cu
	Kazuyoshi Z. Nanjo nanjo@eri.u-tokyo.ac.jp
	Gesa M. Petersen gesap@gfz-potsdam.de
	Danijel Schorlemmer danijel.schorlemmer@gfz-potsdam.de
	Tony A. Stabile tony.stabile@imaa.cnr.it
Opposed Reviewers:	

Evaluation of the event detection level of the Cuban seismic network

Eduardo R. Diez Zaldivar [(1)], Enrico Priolo [(2)], Denis Sandron [(2)], Viana Poveda Brossard [(1)], Marco Cattaneo [(3)], Simone Marzorati [(3)], Raúl Palau Clares [(1)]

[(1)] Centro Nacional de Investigaciones Sismológicas (CENAIS), Santiago de Cuba, Cuba.

[(2)] Istituto Nazionale di Oceanografia e di Geofisica Sperimentale — OGS, Sgonico, Italy.

[(3)] Istituto Nazionale di Geofisica e Vulcanologia (INGV), Osservatorio Nazionale Terremoti, Ancona, Italy.

Corresponding author: Enrico Priolo.

OGS (Istituto Nazionale di Oceanografia e di Geofisica Sperimentale), CRS (Centro Ricerche Sismologiche), Borgo Grotta Gigante, 42/C – 34010 Sgonico (TS), Italy

Phone: +39 040 2140.351

E-mail: epriolo@inogs.it

Declaration of Competing Interests. The authors acknowledge there are no conflicts of interest recorded.

Abstract

The detection level of a seismic network is a measure of its effective ability to record small earthquakes in a given area. It can vary in both space and time, and depends on several factors as meteorological conditions, anthropic noise, local soil conditions —all factors that affect the seismic noise level—, as well as the quality and operating condition of the instruments. The ability to estimate the level of detection is of tremendous importance both in the design of a new network and in determining whether a given network can recognize seismicity consistently, or needs to be improved in some of its parts.

In this paper, we determine the detection level of the Cuban seismic network using the empirically estimated seismic noise spectral level at each station site and some theoretical relationships to predict the signal amplitude of a seismic event at individual stations. The minimum local detectable magnitude thus depends on some network parameters such as the signal-to-noise ratio and the number of stations used in the calculation.

We also demonstrate the effectiveness of our predictions by comparing the estimated detection level with those empirically determined from one year of data (i.e., the year 2020) of the Cuban seismic catalog.

Our analysis shows, on the one hand, in which areas the current Cuban network should be improved, also depending on the regional pattern of faults, and, on the other hand, indicates the magnitude threshold that can be assumed homogeneously for the catalog of Cuban earthquakes in 2020. Since the adopted method can use current measurements of the seismic noise level (e.g., daily), the proposed analysis can also be configured for continuous monitoring of network state quality.

Keywords: Seismic networks, seismic monitoring, earthquake detection level, seismic noise, PQLX, seismicity

Introduction

Estimating the detection capability of a seismic network is of tremendous importance both to design a new network and, for an existing network, to evaluate its performance and define how to improve it. Some of the possible motivations of implementing and performing such a task are: consistent and uniform recognition of the seismicity over the whole target area of monitoring, evaluation of the network setup and possible changes to it in order to achieve a target magnitude of completeness in the resulting earthquake catalog, continuous control of the network operativity and efficiency through the measurement of the acquired data and its overall performance.

The detection capability can be expressed in some different ways. One of them is the magnitude of completeness, which is defined as the lowest magnitude of events that a network is able to record reliably and completely (Schorlemmer & Woessner, 2008). This concept has also been formulated by a probability approach by Nanjo *et al*., (2010). An alternative way is that of estimating the minimum magnitude of earthquakes that can be detected or localized over the target area (e.g., Raymer & Leslie, 2011).

Obviously, when evaluating the detection capability, spatial and temporal errors in event location implicitly play a relevant role and should be assessed independently, to improve the overall estimation of the seismic network performance (Zivcic & Ravnik, 2002; D'Alessandro *et al.*, 2011).

There also are some different and not less important points of view in evaluating the performance of a network, for example that of measuring the amount of time needed to detect an earthquake, an issue which of primary interest for early-warning systems (e.g., McNamara *et al.*, 2016) or that of continuously assessing the quality of the monitoring, as described by Petersen *et al.*, (2019) for the European Alp Array network. However, those issues are quite far from the interest of the present study.

An important concept is that the detection capability is a property that is neither uniform in space nor constant in time. This is due to several causes, such as, for example, instrument operation, the quality of the overall hardware, which can be different among stations and degrade over time, the atmospheric conditions, the anthropogenic noise, and the local soil conditions. All of these factors affect the noise level of the recorded signal, an amount that can be measured and assessed in the spectral domain with an appropriate processing plan.

The Caribbean region has a documented history of natural catastrophes (i.e., hurricanes, volcanoes, earthquakes, and tsunamis) with a high economic cost and human lives losses. The last 500 years of documented history highlight several relevant earthquakes and associated tsunamis, such as the events that occurred in Jamaica in 1692, the Virgin Islands in 1867, Puerto Rico in 1918, Cuba in 1932 and 1992, and the Dominican Republic in 1946. Haiti was the area most affected by earthquakes in this century, with the M_W7.7 event of January 28, 2020, —the largest earthquake recorded in the area since the instrumental age— and other thee moderate-to-strong events (i.e., the M_W7.0 in 2010, M_W5.9 in 2018, and M_W7.2 in 2021, respectively).

The location of the Cuban island right in the middle of the Caribbean Sea is strategic for improving the overall seismic monitoring capabilities in the Caribbean region. As part of regional cooperation, the Cuban Seismological Service offers the data of 19 broadband stations installed in the country and more than 40 accelerographs operating in the southeastern part of Cuba through the service provided by IRIS (2017) and FDSN. Thus, assessing the performance of such a monitoring system, as already done for other networks in the Caribbean area, may contribute to strengthening the overall monitoring system and homogenizing the contributions provided by every single network. In this respect, we mention, among others, the studies performed by: Clinton et al. (2006) with the analysis of the seismic monitoring in Puerto Rico; McNamara et al. (2016), who assessed the performance of the seismic networks installed in the Caribbean

87 region; and De Zeeuw-van Dalfsen and Sleeman (2018) who presented the results of seismic and
88 volcanological monitoring network in the Dutch Antilles.
89 This paper is deeply grounded on the work done by Marzorati & Cattaneo (2016), which
90 developed the software to assess the minimum detectable magnitude of a network and applied it
91 to the Marche-Umbria regions (Italy). However, some other studies are worth being cited for the
92 reader's benefit, as: Greig & Ackerley (2014), who developed a tool to assess the network
93 performance by estimating both location accuracy and magnitude of completeness, and apply
94 this technique to a seismic network located in the New Madrid Seismic Zone (central United
95 States); Franceschina *et al.*, (2015), who assessed the detection capability of a new local network
96 realized for monitoring the CO2 geo-sequestration in the depleted gas storage field of
97 Cortemaggiore (Po Plain, northern Italy); Gestermann *et al.*, (2016), who investigated the spatio-
98 temporal variation of the completeness magnitude in the Northern Germany Basin area, an area
99 which hosts several natural gas field, taking into account the noise levels and geometry of the
100 changing seismic network; McNamara *et al.*, (2016), who estimated the minimum detection
101 magnitude (for moment magnitude M_W) and P-wave detection time for the Caribbean Region.
102 In this paper, we determine the detection level of the Cuban seismic network using the
103 empirically estimated seismic noise spectral level at each station site and some theoretical
104 relationships to predict the signal amplitude of a seismic event at individual stations. We will
105 estimate the distribution of the minimum local detectable magnitude and evaluate the number of
106 triggered stations for a reference magnitude $M_L = 1.0$, which is assumed as a possible future target
107 for the completeness of the Cuban Earthquake catalog. We eventually demonstrate the validity
108 of our predictions by comparing the estimated detection level with those empirically determined
109 from one year of data (i.e., the year 2020) of the Cuban seismic catalog.
110 We think that the analysis and results shown in this paper may have a potential interest wider
111 than just the regional scientific one. On the one hand, the implementation of continuous, or at

least regular, quality control allows network operators to investigate the characteristics of earthquake catalogs better, and, in particular, to avoid attributing possible variability in seismicity rates due to variations in both the seismic network and background seismic noise to active tectonic causes. On the other hand, our procedure can be applied to predict or assess the quality of any seismological network. Let us think in particular of local networks dedicated to monitoring the seismicity of underground industrial activities, for which a level of performance must be guaranteed at the design level and demonstrated later during monitoring operations.

Tectonic environment

Geographically, the Cuba island belongs to the Caribbean region, the area at west of the northern Atlantic Ocean between North and South America. It is a complex region from a geological and tectonic point of view, for which different and sometimes controversial opinions on its evolution have been formulated over time. Figure 1a shows the position of Cuba in the Caribbean tectonic context.

Initially, some authors claimed that Cuba belongs to the North American tectonic plate and that its southeastern edge borders the Caribbean plate (Mann *et al.*, 1995; Lundgre & Russo, 1996; Mann, 1999). This edge approaches a transcurrent fault system parallel to the coast and featuring left lateral movement, known as the "Oriente" (also called "Bartlett-Caimán") fault system zone. This tectonic structure affects not only the territory of Cuba but also other Caribbean islands such as Jamaica, Cayman Islands, Puerto Rico, and Hispaniola.

However, some more recent studies on this plate boundary zone (DeMets, 1990; Deng & Sykes, 1995 and Calais & Lepinay, 1993) have demonstrated, also using arguments based on crustal deformation modeling, the existence of a microplate between the North American and the Caribbean Plates, namely the Gonave microplate, previously proposed by Rosencrantz and Mann (1991) (Figure 1a).

The Gonave microplate is a semi-rectangular microplate that has an area of approximately 190000 km^2 and borders the North American and Caribbean plates to the South and North, respectively (Heubeck *et al*., 1990; Mann *et al*., 2004). The "Oriente" fault zone is responsible for most of the strong earthquakes that occurred in this area, as inferred from the estimation of energy accumulated by the relative movement between the plates described above (Arango, 2009).

Seismicity

Cuba's seismicity features both "interplate" and "intraplate" characters. Interplate seismicity is related to the Oriente fault zone and features a higher frequency of occurrence of earthquakes that can reach large magnitude (M_W > 7.0) and depth greater than 20 km.

More than 90% of the earthquakes that strike the country occur in the southeastern area of Cuba (Alvarez *et al*., 1977, 1991, 1999; Moreno *et al*., 2002). However, some moderate seismicity is also associated with minor faults existing inland of Cuba, which produced some moderate earthquakes with considerable damage (Chuy, 1999).

The map in Figure 1b shows the earthquakes recorded in Cuba (magnitudes between 3.0 and 7.0 on the Richter scale) since the appearance of the instrumental record to the present and highlights the overall seismicity, with both interplate and intraplate earthquakes. The historical earthquakes, although not presented in this map, follow the same tendency in terms of location and estimated magnitude (Chuy, 1999).

Besides the large and moderate earthquakes, it is also important to record the weak seismicity accurately, as it is crucial for defining the seismic regime of the area as a whole, as well as for estimating the accumulation/release of tectonic deformation, the scattering, and attenuation properties of the crust, and the seismic hazard, among other quantities (Arango *et. al.*, 2021). The

map in Figure 2a shows the recorded earthquakes with M_L between 0.4 and 3.0 during the year 2020.

Seismic network

Historical literature dates the deployment of the first geophysical-seismological instruments in Cuba at the beginning of the 20th century, with a Bosch-Omori seismometer in Havana city managed by the Jesuit priests. However, the systematic instrumental seismic recording in Cuba began in 1964, with the installation of the first seismological station in Soroa (SOR), in the western part of the country, followed the next year by the second station in Río Carpintero (RCC), in the southeastern part of Cuba near Santiago de Cuba city (Moreno, 2002a). Both stations, initially equipped with short-period instruments, were the basis for the subsequent development of the Cuban Seismic Survey.

Later, two different stages can be distinguished: the first one, from the mid-1960s to 1997, with the deployment of analog instrumentation mostly equipped with short-period stations and photographic-visual recording (Serrano & Alvarez, 1983); and a second period, from 1998 to the present, characterized by digital instruments, either short-period, broadband, or accelerometric (Diez *et. al*., 1999).

At present, the National Seismological Service (SSN in Spanish) manages 19 broadband digital stations with national coverage, which transmit data in real-time to the Geodynamic Observatory in Santiago de Cuba city. The name of these stations, coordinates, and type of soil on which they are located are shown in Table 1, while their location is indicated in the map in Figure 2b (Diez *et al*., 2014).

The data recorded by the seismic stations are acquired remotely by the SSN Geodynamic Observatory, which hosts the infrastructure designed for the storage and analysis of these signals.

The core of the processing system is a central server equipped with the SeisComP3 software (Helmholtz-Centre Potsdam - GFZ German Research Centre for Geosciences and gempa GmbH, 2008), which is in charge of real-time data acquisition, automatic phase picking, and preliminary estimation of the main parameters of recognized earthquakes (e.g., location, depth, and magnitude). Waveform data are archived in miniSEED format (IRIS, 2022). Offline analysis of the data is performed in parallel manually, to increase the accuracy and detect any seismic event that was overlooked by the automatic system. The two approaches complement each other and improve the quality of the final result. The data of the earthquakes recognized by the Cuban SSN are gathered in an earthquake catalog in SEISAN format (Ottemöller & Havskov, 2014).

In this paper, we use the year 2020 data from the SSN earthquake to validate the results of our analysis. This dataset is provided as a deliverable of this study in the Electronic Supplement. The general SSN earthquake catalog is available for consultation at http://www.cenais.cu.

Method

This study is focused on determining the detection level of the Cuban network, identifying the number of stations that are capable of recording all earthquakes with a small reference magnitude, considered as the minimum detection threshold to be reached in the future.

Different approaches have been applied in Cuba in the past to assess the detection capability of the Cuban seismic network. Alvarez *et al.* (2000) proposed the determination of the detection threshold based on the energetic classes analysis. More specifically, they used the Rautián's *Kr* and *Kd* energetic classes, based the first on the measurements of the P and S waves maximum amplitudes, and the second on the total duration of the earthquake signal, respectively. Gonzales *et al.* (1996) used the magnitude per volume wave (MVP) for the same purpose, while Moreno (2002b) proposes a new detection level from the SEISAN digital format catalog and using the

local magnitude M_L, assuming that the network is homogeneous and that the attenuation of seismic waves is the same in all directions.

All the previous methods were based on the offline processing of the earthquake catalog. However, as nowadays the data acquisition and processing are almost in real-time, some new approaches based on much more massive use of recorded data and empirically measured parameters and allowing a nearly continuous update of the estimations can be implemented.

The approach by Marzorati and Cattaneo (2016) assumes that both the earthquake source and the propagation path can be described theoretically through Brune's spectrum (Brune, 1970) and a suitable spectral attenuation law, respectively, then the seismic noise at each station is the basic observed quantity and it can be expressed as a power spectral density (PSD), according to McNamara & Boaz (2005). As we can calculate theoretically the signal at any station for any given earthquake, the seismic noise level affects directly the observed signal-to-noise ratio (SNR) and influences the detection threshold at each site. Usually, the SNR threshold is set at no less than 2 in seismic network packages, for the frequency band of interest (which depends on the network target).

Two configuration parameters are fundamental for our method to simulate the earthquake detection, as usually carried out by nearly any seismological network software: one is the SNR while the other one is the minimum number of triggered stations for declaring an event. In our simulations, we will test different values for those parameters

The mean (RMS) noise amplitude at each station is calculated independently in the form of a power spectral density (PSD) function; this is performed using the PASSCAL Quick Look eXtended (PQLX) program (McNamara & Boaz, 2005).

The method discretizes the study area into a regular three-dimensional mesh, where each node represents a hypothetical earthquake hypocenter with a certain magnitude. We set a grid-step of

0.015 degree. The theoretical amplitude of the earthquake signal is calculated at each node based on the source-station distance through the so-called attenuation law, which can be defined either empirically or theoretically. In this study, we use the empirical attenuation law currently in use at the SSN of Cuba (Moreno, 2002b). Then, the method calculates the SNR for the current value of noise PSD at each station and selects the triggered stations, i.e., those stations for which the SNR is larger than the assumed threshold. If the number of triggering stations is more than the assumed threshold number, then the event is declared detected and the node is switched on. Those operations are performed for earthquake magnitudes ranging in a selected interval, thus in the end the method provides the answer (YES or NO) on whether an earthquake with a given magnitude occurring on a given location (i.e., a node of the volume) would have been detected or not by the seismic network with the assumed parameter configuration.

The results are represented graphically as isolines in a map, the so-called detection map. As will be shown later, the obtained maps (or isolines) may not be static, that is they may change over time due to local, anthropic, temperature, cultural noise, and other effects. The result depends on how the seismic noise is calculated and interacts with the recorded signal.

Waveform dataset and processing

The geographic area considered in this study is Latitude 15.00°- 28.00° N and Longitude 70°-87° W. It corresponds to the effective coverage area of the Cuban network, designed for the detection of the local and regional earthquakes.

In this study, we used both the waveform recordings and the locations performed by the SSN network during the year 2020. To evaluate the network at its current state of development and to the best of its current performance —this means with all the new sensors and the stabilization of the real-time data transmission—, we use only the last full year of data, i.e., the year 2020. For assessing the seismic network performance, we analyze the continuous waveform data recorded

by each station using a statistical approach, as the signals are mainly composed of a stochastic signal. In particular, data are processed by the PQLX, which is an open-source software package distributed by IRIS (2017) for evaluating the performance of the network seismic station and the quality of the recorded data (McNamara & Boaz, 2005 and 2010). It calculates the Power Spectral Densities (PSD) and the Probability Density Function (PDF) from the full waveform by processing several trace segments having a pre-defined time length and overlap, respectively. The PSDs are stored in a MySQL database which allows a specific series of PSD to be accessed through a user interface.

In addition, PQLX allows the estimation of several statistical parameters, as the mode, the mean, and the expected value at different percentiles (e.g., 10%, 90%, and 95%). As will be discussed below, the determination of the detection capability of the seismic network relies on the use of these parameters

In our study, we used temporal windows of one-hour duration and 50% overlap. Waveform data are first corrected for the instrument response (by deconvolution with the instrument response function), then, they are pass-band filtered in the frequency band 3-15 Hz (0.06 - 0.33 s), which is the band used for the S- and P-phase picking for local earthquakes.

Seismic noise in Cuba

Seismic noise studies in Cuba are recent, due to the availability of relatively large amounts of data and suitable analysis tools only in recent times. The most comprehensive study on seismic noise in Cuba is that of Poveda and Diez (2021), who characterized the seismic noise and its sources for all the stations of the Cuban seismic network.

In general, the Cuban SSN instruments are deployed at the surface and are often affected by high-frequency anthropogenic noise. This can have a negative impact especially in the detection of

low-magnitude local earthquakes, for which the analyzed frequency band is 1 - 20 Hz (i.e., periods 0.05 - 1 s).

In particular, the PSD curves feature two main influencing factors (Poveda and Diez, 2021), i.e., 1) the noise peaks in the period range 2 - 20 seconds due to smaller primary ocean microseism generated in shallow waters in coastal regions together with the secondary ocean microseisms generated by the superposition of ocean waves of equal period traveling in opposite directions (period ranges between 2 and 6 seconds) —a feature which affect nearly all sites as Cuba is an archipelago and therefore all the sites are near the coast—; and 2) the day-night noise variation in the period range 0.05 - 1 s due to both the human activity cycle near urbanized areas and the influence of the wind on the vegetation. On the other hand, the analyses corroborate the little influence of the Cuban natural season cycle, which has two seasons per year, namely the rain and dry season, respectively.

As an example of the cases of extreme noise, Figures 3 shows the PDF curves for the vertical component of the "Cascorro" (CCCC) and "Caibarién" (CAIB) stations, respectively. The red rectangle indicates the period band analyzed in this study.

However, all the PSD curves obtained for the Cuban SSN stations are within the range established by Peterson's models (Peterson, 1993), see Electronic Supplement Figure S1, so it can be concluded that almost all sites have an acceptable noise level according to the current seismology standard.

Estimation of noise amplitude from PSD values

The method by Marzorati & Cattaneo (2016) determines the detection level by comparing the earthquake signal amplitude to the actual noise amplitude through their ratio (i.e. the signal-to-

noise ratio SNR). The noise is provided as an input to the program in terms of a PSD function, which has already been calculated by the PQLX program.

However, as we have to compare the amplitude of the earthquake signal with that of the background noise, we need to convert the PSD into a corresponding waveform amplitude defined in time domain. For doing that, we follow the approach proposed by Aki and Richards (1980) and Bormann (2002). If we consider the signal energy concentrated in a limited frequency band [f_1, f_2], the maximum amplitude of a wave *f(t)* near $t = 0$, can be determined approximately by the product of the so-called "energy spectral density" with the wave bandwidth, as shown in equation (1):

$$f(t)_{t=0} = |F(\omega)|2(f_2 - f_1) \tag{1}$$

where $F(\omega)$ is the representation of the arbitrary transient function in the frequency domain *f(t)* according to Fourier integral transformation.

Using the Fourier transformation property (Parseval's theorem), the energy spectral density is expressed as:

$$\int_{-\infty}^{\infty} f(t)^2 dt = \int_{-\infty}^{\infty} \frac{|F(\omega)|^2}{2\pi} d\omega = \int_{-\infty}^{\infty} |F(2\pi v)|^2 dv \tag{2}$$

where we have the total energy of signal *f(t)* (proportional to the physical energy) on the left side, while the integrand on the right side represents the energy spectral density.

On the other hand, as seismic noise is a stationary random signal, instead of a transient signal, and have infinite energy but finite power, it is more appropriate to substitute the concept of power spectral energy with that of power spectral density (PSD), which represents the energy spectral density per unit time. Then, we can write the mean square amplitude of noise in the time domain as follows:

$$< f^2(t) >= 2P(f_2 - f_1) \tag{3}$$

where P is the signal power and is obtained by integrating the power spectral density PSD over the frequency band [f_1, f_2].

The noise amplitude, which is usually written as root mean square (RMS) of the signal, is then obtained as:

$$A_{RMS} = \sqrt{2P\,(f_2 - f_1)} \qquad (4)$$

The A_{RMS} value of equation (4) is the actual noise amplitude which is used to calculate the SN ratio.

Results and discussions

We estimate the detection capability of the Cuban seismic record using the approach by Cattaneo and Marzorati (2016). We chose the PSD "Mode" as a statistical parameter representing the noise level observed at each station. This parameter was extracted, for each station, as the average of the whole set of frequency-dependent Mode values calculated day-by-day for the year 2020.

We set at 2 the minimum SNR value for an event that can be detected. Moreover, to comply with the SeisComP3 setting for automatic earthquake detection, we set that at least three stations have to be triggered (i.e., their SNR must be greater than 2) to declare an event as a possible earthquake candidate.

In Figure 4, we show the results of two scenarios. In the first one, we assess the overall detection capability of the network in a very favourable condition, i.e. a tolerant signal-to-noise ratio threshold of SNR = 2 and event declaration for a minimum of 3 triggered stations. In the second scenario, we assume a target magnitude of M_L = 1.0 for the Cuban grid and calculate, for each grid point, how many stations would be able to detect such an earthquake occurring at that point.

It can be seen that for the eastern part of the country, the network should be able of detecting earthquakes with a minimum magnitude M_L = 1.0 (Figure 4a). This is a suitable value for both

real-time seismic monitoring and detection of the overall seismicity, respectively, which are the objectives for which the network was designed. The situation worsens significantly in the central-western part of the island, where there are much less stations, and those stations are often deployed in noisy sites. In those areas, the minimum magnitude of detection rises from M_L = 1.2 to even M_L = 2.5 in the extreme part to the West. In practice, $M_L \approx 2.0$ is the minimum detectable magnitude for accurately localized earthquakes (i.e. determined by at least 3 stations) occurring over 99% of the Cuban territory.

This minimum level of detection is mainly influenced either by the poor quality of some station sites or the installed instruments. Among the latter, we mean sensors deployed on the ground surface and lacking thermal and/or electrostatic insulation, a solution particularly sensitive to natural or anthropogenic noise. A fairly high level of noise along with the occurrence of spurious signals also affects some of the stations recently installed to densify the network (Poveda and Diez, 2021).

Figure 4(b) shows the total number of stations that would detect a weak (i.e., M_L = 1.0) earthquake. While in the eastern part of the island, where the Cuban network is dense, a weak earthquake would be detected by 6 to 10 stations, in the rest of the country, from the middle to the extreme west of the island but a small area, an M_L = 1.0 earthquake would hardly be detected by at least 3 stations and it would even be outside the coverage range of the network. However, even some parts of the eastern part of the island suffer of poor coverage. For example, a weak earthquake occurring offshore the Cabo Cruz area (i.e. around latitude 20° N and longitude 78-79° W; see yellow star in Figure 4b) would be detected only by few stations (e.g., PILO and LMGC) and this would affect negatively the location quality.

To assess the overall detection capability of the network, we assume a bad condition characterized by a high level of seismic noise, a situation that occurs, for example, during atmospheric disturbances or hurricanes that cause strong winds and ocean waves. To simulate

this behavior we use the statistical parameter "95% of the PSD" in our calculation; other parameters, such as the SNR, are maintained the same. The results are shown in Figures 5.

Figure 5(a) shows that under bad noise conditions the area where the target magnitude M_L = 1.0 is detected reduces considerably: while the eastern part of Cuba still meets this condition, in the rest of the territory, the minimum detected magnitude rises to 1.5 in a large area and reaches 2.4 in the westernmost part of the island. Figure 5b shows the eastern part of Cuba in greater detail: the central part of the region satisfies the target homogeneously, instead the minimum detected magnitude worsens to M_L = 1.3 - 1.4 towards the two extreme tips to West (in the Cabo Cruz-Pilon area) and East (in the neighborhood of the MASC station), respectively. Note that the eastern area of Cuba is of particular interest for detecting earthquakes occurring in Haiti, the Dominican Republic, and in the ocean channel (named "Paso de los Vientos") between the islands of Cuba and Haiti, respectively.

On the other hand, Figure 5c shows that under bad noise conditions the target magnitude M_L = 1.0 would trigger only one station in a large part of the country and only the eastern part of Cuba would detect an M_L = 1.0 earthquake by 3 triggered stations.

In conclusion, the estimated performance shows that the Cuban seismic network meets the minimum request of being able to localize the seismicity in the most seismic area near the island, i.e. the Oriente fault system, while it is insufficient to detect and localize with adequate accuracy the low-level seismicity that occurs throughout the archipelago (see Figure 1a).

Earthquakes detected by one station

About one-third of the earthquakes recorded annually in Cuba and reported in the SSN earthquake catalog are recorded by only one station and are detected through the manual analysis carried out by seismologists. Many of those earthquakes have magnitude M_L < 1.0 and are relevant for studying weak seismicity. For this reason, we assess the detection capability of the

Cuban network based on single-station triggers. The results are presented in Figure 6, in terms of minimum detected magnitude (panel a) and number of triggered stations for a magnitude M_L = 0.2 earthquake (panel b), respectively). Looking at both maps together, it is evident that small earthquakes (i.e. down to M_L = 0.2) can be detected in the whole south-eastern part of Cuba, however, they will be localized accurately only in a small region (area colored in sky blue, green, or orange), while in the rest of the island they will be detected mainly by one single station. For about two-thirds of the national territory it is impossible to detect earthquakes below M_L = 1.0 using automatic analysis tools, a condition that limits heavily any study of intra-plate low-energy seismicity.

The main way to improve the detection performance of the network is to increase the number of stations in the western part of the island in the future and choose suitable sites; however, some other actions can help to improve the quality of the existing stations, such as deploying posthole or borehole seismometers and ensuring adequate thermal and electromagnetic isolation of the seismometer.

Validation

To validate our study, we compare the results of our predictions with data from the earthquake catalog. We focus on the number of triggered stations in the case of small earthquakes, i. e. earthquakes with M_L near to 1.0, which is assumed as a target of completeness for our network. We also restrict this analysis to the eastern part of Cuba since the higher concentration of earthquakes around the Oriente fault zone results in a larger volume of observed data. To get comparable results, we applied the following selection criteria for building the datasets: for the theoretical estimations, SNR = 2 and a minimum of 3 triggered stations minimum to declare an event; for the observed data, we extracted from the 2020 seismic catalog (CENAIS, 2020) earthquakes with M_L between 0.9 and 1.1 and, for these earthquakes, the number of triggered

stations. In Figure A1 of Appendix 1, we show both the map of the whole 2020 catalog and that of the events with $0.9 \leq M_L \leq 1.1$ localized in the eastern part of the island (panels a and b, respectively). For each event, the color corresponds to the number of triggered stations.

The maps of Figure 7 compare the number of triggered stations assessed from the observed data (panel a) with those estimated theoretically (panels b - d). For the observed data, the map was obtained through spatial interpolation using the "near-neighbor" algorithm of the GMT software package (Wessel et al, 2013). This algorithm assigns to each node of the grid the weighted average of the values of the nearest data belonging to a circular neighborhood with radius R. The map of Figure 7a was obtained by setting R = 50 km and by dividing the circular neighborhood in 6 sectors. More details can be found in the GMT documentation (GMT, 2021).

The map obtained from experimental data (Figure 7a) shows that an earthquake of approximately M_L = 1 is detected by a maximum of 6 - 7 stations in a large area of the eastern island, while the number of triggered stations reduces to 1 - 2 in some restricted areas, namely in the extreme areas to West and East of the southern coast and in a small area of the northern coast, respectively.

The maps shown in Figures 7(b-d) represent the theoretical results of the number of stations triggered by an $M_L \approx 1.0$ earthquake obtained for SNR values ranging from 3 to 5, respectively. A more complete set of maps for a wider range of SNR and number of stations' combinations is shown in the Electronic Supplement, Figures S2 and S3.

Figure 7 quantifies clearly what is intuitively expected, that is that the number of triggered stations decreases when the SNR requested for declaring a trigger increases. This confirms the great importance of this parameter for determining the network performance.

The theoretical map of Figure 7(d), which represents the results obtained for SNR = 5, has high coherency with that of Figure 7(a), which represents the 2020 catalog data. Some minor inconsistencies may be due to several reasons, such as 1) the fact that the assumed noise level

estimated from the annual average of several PSD curves (approximately 17000 per year) does not match the noise level that actually occurs during each event; 2) the fact that, while the theoretical calculation includes only stations from the Cuban seismic network, the 2020 catalog was constructed by using also some stations belonging to other networks in the Caribbean area; and, 3) the lack of actual earthquakes in some parts of the study area, compared with the fact that the theoretical method calculates a theoretical amplitude at each station from a uniform network of points.

In any case, our results obtained for the Cuban network confirm that our method can successfully estimate the detection capability of a seismic network from the measured noise levels at each station. Moreover, the obtained results are good enough to identify the weak elements of a seismic network and help to define some strategies for its improvement.

Conclusions

In our study, we have estimated the detection capability of the Cuban seismic network and validated our estimations with the data of the Cuban 2020 earthquake catalog. We can draw the following conclusions.

At present, with the existing technological infrastructure of the Cuban seismic network, an $M_L \approx 1.0$ earthquake can be detected by at least 3 stations only if it occurs in the eastern part of the country or in some restricted areas of the center or the west of the island. Any $M_L \approx 1.0$ (or larger) earthquake occurring on the Cuban territory or near to it triggers at least 1 station of the Cuban network. Our study suggests that $M_L \approx 2.0$ is the minimum detectable magnitude for accurately localized earthquakes (i.e., determined by at least three stations) occurring over 99% of the Cuban territory, the only exception being the westernmost extreme of the island. To reach a homogeneous capability of detection of an $M_L \approx 1.0$ earthquake (assumed as a target of minimum

magnitude) over the whole Cuban territory the network should be densified in the central and western areas of the country.

The background seismic noise is the factor that mostly affects the overall network performance, and the detection threshold worsens significantly (i.e. the minimum detected magnitude increases) with the increase of the seismic noise level. This may be due to several causes. Some of them are out of human control, such as bad atmospherical or ocean conditions. Others, as the station location and site conditions, are strictly related to a human choice and therefore the background seismic noise can be reduced by some suitable actions, such as using posthole/borehole instruments, providing a correct thermal and electromagnetic isolation of the instruments, or ultimetely moving the station to a better location. Figure S1 reports the PSD of all stations of the Cuban seismic network. At visual analysis, the following six stations should be improved for different reasons: CAIB (a), CAMR (b), CHIV (d), CJAG (e), MARV (h), and PILO (l).

Our study has been successfully validated by comparing the theoretical estimations in terms of number of triggered stations for an M_L = 1.0 earthquake with those obtained for the 2020 earthquake catalog.

The applied method turns out to be a practical and effective way also for evaluating the performance of a seismic network, including how it changes in time —a feature that we have not explored in this paper—, and offers a wide range of automation possibilities in conjunction with some well known seismological software such as SeisComP3 and PQLX.

The location of the Cuban island right in the middle of the Caribbean Sea can provide a strategic contribution to improve the performance of the Caribbean monitoring system, with relevant outcomes for both the alert system and the study of the seismicity on a regional scale. Not only is the Cuban territory adjacent to some relevant active structures, such as the Oriente fault system, but it also is a privileged observatory for the Haiti seismicity —an area still poorly covered by

seismic stations— and in general for depicting the image of the seismicity of the whole Caribbean region. Our study suggests, on one hand, the directions for improving the monitoring capability, and, on the other hand, it indicates the magnitude threshold that can be assumed homogeneously for the 2020 Cuban earthquake catalog.

Data and Resources

The Cuban Seismic Network (SSN; www.cenais.cu; last accessed August 2021 - Rev. Fac. Ing. UCV, Jun 2014, vol.29, no.2, p.69-77. ISSN 0798-4065) is managed by the National Centre for Seismological Research (CENAIS) of the Cuban Ministry of Science, Technology and Environment (CITMA).

The SSN data are freely available from the CENAIS Archive System of Instrumental Seismology (www.cenais.cu/cenais/192.168.12.253/webinterface/; last accessed August 2021). All stations are registered at the FDSN (International Federation of Digital Seismograph Networks, http://www.fdsn.org/; last accessed August 2021).

The following software systems were used: SEISAN (Ottemoller and Havskov, 2014; available at https://www.uib.no/en/rg/geophysics/54592/software#seisan; last accessed August 2021); GMT - Generic Mapping Tools (Wessel and Smith, 1991; Wessel et al., 2013; available at http://gmt.soest.hawaii.edu/; last accessed August 2021); AWK (Aho et al., 1987), with its GNU implementation GAWK (available at www.gnu.org/software/gawk; last accessed August 2021); PQLX (McNamara and Boaz, 2010; avialble at https://www.usgs.gov/software/pqlx-a-software-tool-evaluate-seismic-station performance; last accessed August 2021); and MATLAB, version 9.0.0 (R2016b), Natick, Massachusetts: The MathWorks Inc. (https://www.mathworks.com/products/matlab.html. last accessed, August 2021).

This article is accompanied by an Electronic Supplement, which includes the following material: the Cuban 2020 earthquake catalog (Data Set DS01); the probability density functions calculated

from the continuous recordings of seismic noise for all stations of the Cuban seismic network (Figure S1); the estimated detection levels of the Cuban seismic network in terms of minimum detected magnitude (Figures S2) and the number of triggered stations for an M_L 1.0 earthquake hypothetically located at each point study area (Figure S3), respectively.

Acknowledgments

We acknowledge the full collaboration of the colleagues from the Cuban National Seismological Centre during various stages of our research; we especially thank Mrs. Maribel Leyva Arias and Mr. Enrique Arango for their help in extracting data from the seismic catalog and for their quick help in solving the problems derived from the selection of the data that were used in this study. This research was mainly carried out during some visiting periods of Eduardo Diez Zaldivar at OGS, in Italy. Those visits were partially supported by the Abdus Salam International Center for Theoretical Physics (ICTP), within the Training and Research in Italian Laboratories program (TRIL); we thank ICTP for the excellent support provided for arrnanging all the aspects of the visits. Even if not cited explicitly in the text, this study was also motivated by the need of assessing the detection performance of two local seismic networks managed by OGS for the seismic monitoring of two underground gas storages located in Northern Italy at Collalto (Veneto Region) and Cornegliano Laudense (Lombardia Region), respectively; in this regard, we acknowledge that this study was partially funded by Edison Stoccaggio S.p.A., the storage concession holder, under contract n. 1500118977 CO established between Edison Stoccaggio S.p.A. and OGS on 11 December 2019, and by Ital Gas Storage S.p.A., under a research contract established among Ital Gas Storage S.p.A., OGS, and CNR-IREA on 16 February 2018, respectively. Finally, we would like to thank the two reviewers (Thomas Braun and an

anonymous reviewer) and Editor-in-Chief Allison Bent for their thorough review, and clear and constructive suggestions, which helped us improve our manuscript considerably.

References

Aho, A.V., Kernighan, B. W., and Weinberger, P. J. (1987). The AWK programming language. Addison-Wesley Longman Publishing Co., Inc.75 Arlington Street, Suite 300 Boston, MA, United States. ISBN: 978-0-201-07981-4. 210 pages.

Aki K. & Richards P. G. 1980. Quantitative Seismology, Theory and Methods. Volume I: 557 pp., 169 illustrations. Volume II: 373 pp., 116 illustrations. ISBN 0 7167 1058 7 (Vol. I), 0 7167 1059 5 (Vol. II).

Álvarez, J.L. and Bune,V.I. 1977 Estimación de la peligrosidad sísmica de la región suroriental de Cuba. [en ruso]. Fizika Zemli, No.10, pp. 54 - 67.

Álvarez, L. Chuy, T. and Cotilla, M. 1991 Peligrosidad sísmica de Cuba. Una aproximación a la regionalización sísmica del territorio nacional. Revista Geofísica No 35, pp.125-150.

Álvarez, L., Chuy, T., García, J., Moreno, B., Álvarez, H, Blanco, M., Expósito, O., González, O., Fernández, A.I. 1999 an earthquake catalogue of Cuba and neighbouring areas. ICTP internal report ic/ir/99/1, Miramare, Trieste, Italy, 60 p.

Arango, *et al.*, 2009. Análisis geodinámico y sismotectónico del extremo oriental de Cuba. Acta GGM Debrecina. Vol 4, pp 43-52.

Arango, E., D. 2014. Análisis sismotectónico del territorio oriental de Cuba a partir de la integración del modelo de corteza 3D de datos gravimétricos con datos sismológicos y geodésicos. Tesis doctoral. Centro de Investigación científica y de Educación Superior de Ensenada, Baja California, México.

572 Arango, *et al.*, 2021. Sismicidad Registrada en el territorio nacional y estado de la red de
573 estaciones del servicio sismológico nacional. Vicedirección Técnica. Archivos de
574 Centro Nacional de Investigaciones Sismológicas, Ministerio de Ciencia, Tecnología y
575 Medio Ambiente, 2020.
576 Bormann, P. *et al*. IASPEI New Manual of Seismological Observatory Practice (NMSOP),
577 2002.
578 Brune, J.N. (1970). Tectonic stress and spectra of seismic shear waves from earthquake, J.
579 Geophys. Res., 75, 4997-5009.
580 Calais, E., Lépinay, M. 1989. Géométrie et régime tectonique le long d une limite de plaques en
581 coulissage: la frontiére nord-Caraïbe de Cuba á Hispaniola Grandes Antilles.
582 Géodynamique. C R. Acad. Sci. Paris, t. 308, serie II, pp 131-135.
583 Calais, E., Lépinay, M. 1993. Semiquantitative modeling of strain and kinematics along the
584 Caribbean/North America strike-slip plate boundary zone. Tectonophysics, J.
585 Geophys. Res. Vol. 98. N B 5, pp. 8 293 - 8 308.
586 CENAIS. 2020. Catálogo de terremotos (extracción parcial del año 2020 del catalogo general
587 de terremotos). Fondos del CENAIS.
588 Chuy, T. 1999. Macrosísmica de Cuba y su aplicación en los estimados de peligrosidad y
589 microzonación Sísmica. Tesis en opción al Grado de Doctor en Ciencias Geofísicas.
590 Fondos del MES y CENAIS. 150 p.
591 Clinton, J., G. Cua, V. Huérfano, C. von Hillebrandt-Andrade, and J. Martinez Cruzado (2006).
592 The current state of seismic monitoring in Puerto Rico, Seismol. Res. Lett. 77, 532–
593 543.
594 DeMets Ch. 1990. Earthquake slip vectors and estimates of present-day plate motions. Journal
595 of geophysical Research, Vol. 98, No. B4, pp. 6703-6714.

596 Deng J, and Sykes L. (1995): Determination of Euler polo for contemporary relative motion of
597 Caribbean and North American plates using slip vectors of interpolate earthquakes.
598 Tectonics. Vol. 14, No 1, pp. 39 - 53.
599 Diez, E., 1999. Cuban National Seismo-telemetric network, Abdus Salam Internacional Centre
600 for Theoretical Physics (ICTP), Preprint 1999038.
601 Diez, E. *et al*. 2014. Modernización de la red sísmica cubana. Instalación, calibración y puesta
602 a punto. Revista de la Facultad de Ingeniería Universidad Central de Venezuela, 2014,
603 29(2), pp. 69-78, ISSN 0798-4065.
604 D'Alessandro, D Luzio, G D'Anna, G Mangano (2011). Seismic network evaluation through
605 simulation: An application to the Italian National Seismic Network. Bulletin of the
606 Seismological Society of America. Volume 101, Number 3 Pagine 1213-1232.
607 De Zeeuw-van Dalfsen, E., and R. Sleeman (2018). A Permanent, Real-Time Monitoring
608 Network for the Volcanoes Mount Scenery and The Quill in the Caribbean
609 Netherlands. Geosciences, 8(9), 320; https://doi.org/10.3390/geosciences8090320
610 Franceschina G., P. Aaugliera, S. Lovati, and M. Massa (2015). Surface seismic monitoring of
611 a natural gas storage reservoir in the Po Plain (northern Italy). Boll. Geofis. Teor.
612 Appl., 56(4), 489-504; DOI 10.4430/bgta0165
613 Gestermann N., T. Plenefisch, T. Kraft, and M. Herrmann (2016). Seismic network detection
614 capability within the natural gas fields in Northern Germany, ESC General Assembly
615 2016, Trieste (Italy), ESC2016-511, Poster
616 GMT (2021). The Generic Mapping Tools Documentation. The GMT Team.
617 https://docs.generic-mapping-tools.org/latest/#.
618 Greig W. and N. Ackerley (2014) Microseismic Network Performance Estimation: Comparing
619 predictions to an earthquake catalogue. EGU General Assembly Conference 2014,
620 Geophys. Res. Abstracts, Vol. 16, EGU2014-6361.

621 Helmholtz-Centre Potsdam - GFZ German Research Centre for Geosciences and gempa GmbH
622 (2008). The SeisComP seismological software package. GFZ Data Services. doi:
623 10.5880/GFZ.2.4.2020.003.
624 Heubeck, C. and Mann, P. 1991. Geologic evaluation of plate kinematic models for the North
625 American-Caribbean plate boundary zone. Tectonophysis. Vol. 191, pp. 1 - 26.
626 IRIS (2017). Software Downloads – PQLX. Incorporated Research Institutions for Seismology,
627 https://ds.iris.edu/ds/nodes/dmc/software/downloads/pqlx/ (last accessed, February 16,
628 2022).
629 IRIS (2022). miniSEED. . Incorporated Research Institutions for Seismology,
630 https://ds.iris.edu/ds/nodes/dmc/data/formats/miniseed/ (last accessed, February 16,
631 2022).
632 Lundgren P. R., Russo R.M.1996. Finite element modelling of crustal deformation in the North
633 America-Caribbean plate boundary zone. - Journal of Geophysical Research, v. 101,
634 No B5, pp 11317-11327.
635 Mann, P. Taylor, F. Edwards, R. and Ku, T-L. (1995). Actively evolving microplate formation
636 by oblique collision and side-ways motion along strike-slip faults: An example from
637 the northeastern Caribbean plate margin. Tectonophysics. Vol. 246, pp. 1-69.
638 Mann, P. (1999). Caribbean sedimentary basins: Classification and tectonic setting. In: Mann,
639 P. (Ed.), Sedimentary Basins of the World, 4, Caribbean Basins, Elsevier Science
640 B.V., Amsterdam, pp. 3-31.
641 Mann, P., E. Calais., V. Huérfano (2004). Earthquake shakes big bend region of North America
642 Caribbean boundary zone, EOS, Transactions, American Geophysical Union, 85, 24 p.
643 Marzorati, S. and Cattaneo, M. 2016. Stima automatica della magnitudo minima rilevabile
644 dalla rete sismica ReSIICO – Automatic magnitude detection of the seismic network

ReSIICO, Quaderni di Geofisica 2016, Istituto Nazionale di Geofisica e Vulcanologia (INGV), ISSN 1590_2595, 21 pp. (in italian).

McNamara, D.E. and Boaz, R.I. (2005). Seismic Noise Analysis System Using Power Spectral Density Probability Density Functions: A Stand-Alone Software Package. Open-File Report 2005-1438, U.S. Department of the Interior, U.S. Geological Survey.

McNamara, D.E. and Boaz, R.I. (2010). PQLX: A seismic data quality control system description, applications, and user's manual. Open-File Report 2010-1292. doi.org/10.3133/ofr20101292.

McNamara, D.E., Von Hillebrandt-Andrade, C., Saurel, J.M., Huerfano, V. and Lynch, L. (2016). Quantifying 10 Years of Improved Earthquake Monitoring Performance in the Caribbean Region. Seismological Research Letters Volume 87, Number 1 January/February 2016. doi: 10.1785/0220150095.

Moreno, B. (2002a). The new Cuban seismograph network, Seis. Res. Lett., 73, 504-517.

Moreno, B. (2002b). New magnitude scales and attenuation relation for eastern Cuba, in Ph.D. Tesis: Crustal structure and seismicity of Cuba and Web-based applications for earthquake analysis. University of Bergen, Norway.

Moreno, B., Grandison, M. and Atakan, K. (2002). Crustal velocity model along the southern Cuba margin. Implications for the tectonic regime at an active plate boundary. Geophys. J. Int., 151, pp 632–645.

Nanjo, K.Z., D. Schorlemmer, J. Woessner, S. Wiemer, and D. Giardini (2010). Earthquake detection capability of the Swiss Seismic Network, *Geophys. J. Int.,* **181**(3), 1713–1724.

Ottemoller, V., and J. Havskov (2014). Seisan earthquake analysis software for Windows, Solaris, Linux and Macosx, 2014.

Petersen G. M., S. Cesca, M. Kriegerowski, and the AlpArray Working Group (2019). Automated Quality Control for Large Seismic Networks: Implementation and Application to the AlpArray Seismic Network. Seis. Res. Lett., 90 (3): 1177–1190, DOI: https://doi.org/10.1785/0220180342

Peterson J. (1993). Observation and modelling of seismic background noise. USGS, Open file Report 93-322, 95 pp.

Poveda, V., and E. Diez (2021). Ambient noise level in Cuba: Analysis of broadband seismic stations in the Cuban seismic network, Submited to: REVISTA DYNA, Universidad Nacional de Colombia (Sede Medellín). Facultad de Minas, ISSN Impreso: **0012-7353.**

Rosencrantz, E., and P. Mann (1991). SeaMARC II mapping of transform faults in the Cayman Trough, Caribbean Sea Geology 19(7): pp 690–693.

Schorlemmer, D. and Woessner, J., 2008. Probability of detecting an earth- quake, *Bull. Seism. Soc. Am.*, **98**(5), 2103–2217.

Serrano, M.; Álvarez, L. (1983): Desarrollo de la sismología instrumental en Cuba. Investigaciones Sismológicas en Cuba, No. 4, pp. 5-20.

Wessel, P., and W. Smith (1991). Free software helps map and display data, Eos Trans. AGU 72, 441–461.

Wessel, P., W. H. F. Smith, R. Scharroo, J. F. Luis, and F. Wobbe (2013). Generic Mapping Tools: Improved version released. AGU, EOS Trans, 94, 409-410. DOI: 10.1002/2013EO450001.

Zivčić, M., and Ravnik, J. (2002). Detectability and earthquake location accuracy modeling of seismic networks, IS 7.4. In P. Bormann (Ed.), New Manual of Seismological Observatory PracNce (Vol. 1). Potsdam: GeoForschungsZentrum.

695 **Full Addresses**

696 Eduardo R. Diez Zaldivar.

697 Viana Poveda Brossard.

698 Raul Palau Clares.

699 Centro Nacional de Investigaciones Sismológicas (CENAIS)

700 Calle 17 Nro. 61 e/ 4 y 6

701 Reparto Vista Alegre

702 CP 90400, Santiago de Cuba, Cuba

703 diez@cenais.cu

704 viana@cenais.cu

705 rpalau@cenais.cu

706

707 Enrico Priolo.

708 Denis Sandron.

709 Istituto Nazionale di Oceanografia e di Geofisica Sperimentale — OGS

710 Centro di Ricerche Sismologiche

711 Borgo Grotta Gigante 42/c

712 34010 Sgonico, Trieste, Italy

713 epriolo@ogs.it

714 dsandron@ogs.it

715

Marco Cattaneo

Simone Marzorati

Istituto Nazionale di Geofisica e Vulcanologia (INGV)

Osservatorio Nazionale Terremoti

via di Colle Ameno, 5

60126 Ancona, Italy

marco.cattaneo@ingv.it

simone.marzorati@ingv.it

List of Figures & Tables

Table 1. Details of the stations of the Cuban seismic network.

Figure 1. The Cuba island in the Caribbean tectonic context. (a) The main fault systems (red lines; red arrows represent the fault relative movement), with the Bartlett-Cayman fault system (Oriente) and other relevant fault systems in the region (Mann *et al*., 1995; Lundgre & Russo, 1996; Mann, 1999; Mann et al., 2004). (b) Seismicity in Cuba and surrounding areas from 1965 to 2020, taken from the CENAIS historical general catalog and reprocessed for this study by Arango *et. al* (2021). The magnitude range from 3 to 7 is considered (see colors in the legend). We used local magnitude M_L for magnitude not exceeding 5, and moment magnitude M_W for stronger events.

Figure 2. Seismicity of the year 2020 in Cuba and location of the Cuban SSN stations. (a) Map of the earthquakes in 2020 in Cuba and surrounding areas and the location of seismological stations used in this study (black triangles). The magnitude ranges from 0.4 to 7.7 (see colors in the legend). Other details as in Figure 1. (b) Zoom of the previous map emphasizing the eastern part of Cuba.

Figure 3. PDF plots resulting from the analysis of the continuous seismic noise recording for the two extreme cases of the Cuban network in terms of seismic noise. (a) "Cascorro" station (CCCC), which features the lowest seismic noise level and represents the best case. (b) "Caibarién" station (CAIB), which features the highest seismic noise level and represents the worst case. The black box indicates the band period used in the study. The gray lines represent the reference Low-Noise and High-Noise Models (LNM and HNM, respectively) (Peterson, 1993). The other lines represent the other estimated statistical parameters, namely the mode (solid black line), the mean (dashed black line), and the expected value at 10%, 90%, and 95% percentiles (two dashed white lines and solid white line, respectively).

Figure 4. Estimated detection capability of the Cuban seismic network for an average scenario, i.e. using the statistical parameter "Mode of the PSD". A SNR-tolerant condition of SNR=2 for all stations is assumed. The red triangles represent the seismological stations of the network. The Oriente fault is explicitly shown (black line). (a) The spatial detection magnitude for at least 3 triggered stations, which corresponds to the minimum number for classical locations. (b) The number of triggering stations for an M_L1.0 earthquake. The yellow star indicates a weak earthquake occurring offshore the Cabo Cruz area referenced in the text.

Figure 5. Estimated detection capability of the Cuba seismic network in the worst-case statistical scenario, i.e. using the statistical variable "95% of the PSD". A SNR-tolerant condition of SNR=2 for all stations is assumed. (a) The spatial detection magnitude for at least 3 triggered stations which corresponds to the minimum number for classical locations. (b) The number of triggering stations for an M_L 1.0 earthquake. Other details as in Figure 4.

Figure 6. Estimated detection capability of the Cuba seismic network for the limit-case scenarios of further manual inspection. These scenarios represent the maximum expected performance for weak earthquakes. The maps represent the average statistical scenario obtained using the statistical variable "mode of the PSD" , and a SNR-tolerant condition of SNR=2 for all stations, respectively. (a) The spatial detection magnitude for at least 1 triggered station. (b) The number of triggering stations for an M_L0.2 earthquake. Other details as in Figure 4.

Figure 7. Comparison between the theoretical estimations calculated in this study and the experimental data from the CENAIS 2020 earthquake catalog. (a) Number of stations triggered by a earthquake with a magnitude M_L in the range 0.9-1.1, as inferred from the CENAIS 2020 earthquake catalog. The black dots represent the epicenters of the earthquake catalog. (b-d) Estimated number of stations triggered by an M_L1.0 earthquake for different SNR values. (b) SNR=3. (c) SNR=4. (d) SNR=5. Other details as in Figure 4.

Figure A1. Seismicity of the year 2020 in Cuba and surrounding areas, extracted from the CENAIS catalog and corresponding to the data of the 2020 earthquake catalog delivered as Data Set DS01. (a) All earthquakes recorded in 2020. (b) Events with $0.9 \leq M_L \leq 1.1$ localized in the eastern part of Cuba. For each event, the color corresponds to the number of the triggered stations. Black triangles: location of the seismic stations.

785 **Table 1**

Table 1

Cuban seismic network stations characteristics

Station name	Network code	Station code	Latitude (N)	Longitude (W)	Type of soil
Chivirico	CW	CHIV	19.9764	76.4151	Volcanic ash forming layers or strata
Caibarién	CW	CAIB	23.0617	81.3708	Limestones stratified in small layers
Camarioca	CW	CAMR	22.4970	79.4709	Sedimentary Rocks
Cascorro	CW	CCCC	21.1934	77.4173	Very hard igneous rocks (granite)
Holguín	CW	HLG	20.9200	76.2361	Igneous rocks (streamers)
Jaguey	CW	CJAG	22.2683	81.2763	Massive karst limestones deep caverns
Las Mercedes	CW	LMGC	20.0646	77.0045	Volcanic ash forming extracts
Nuevo mundo	CW	NMDO	20.5598	77.4173	Igneous rocks (streamers)
Mar Verde	CW	MARV	20.0052	75.9065	Igneous rocks (basalts)
Maisí	CW	MASC	20.1755	74.2312	Sed. Rock (calcified hard limestones)
Manicaragua	CW	MGV	22.1144	79.9796	Metamorphic rocks weathered soil
Pilón	CW	PILO	19.9140	77.4085	Stratified volcanic rocks
Pinares Mayarí	CW	PIN	20.4855	75.7915	Streamers
Quimbuelo	CW	QMBU	20.1989	74.8127	Compact clusters
Rio Carpintero	CW	RCC	19.9950	75.6965	Very hard igneous rocks
Sabaneta	CW	SAB	20.3418	75.3593	Stratified limestones
Soroa	CW	SOR	22.7932	83.0086	Sedimentary Rocks
Yarey	CW	YAR	20.3577	76.3635	Basalt Rocks

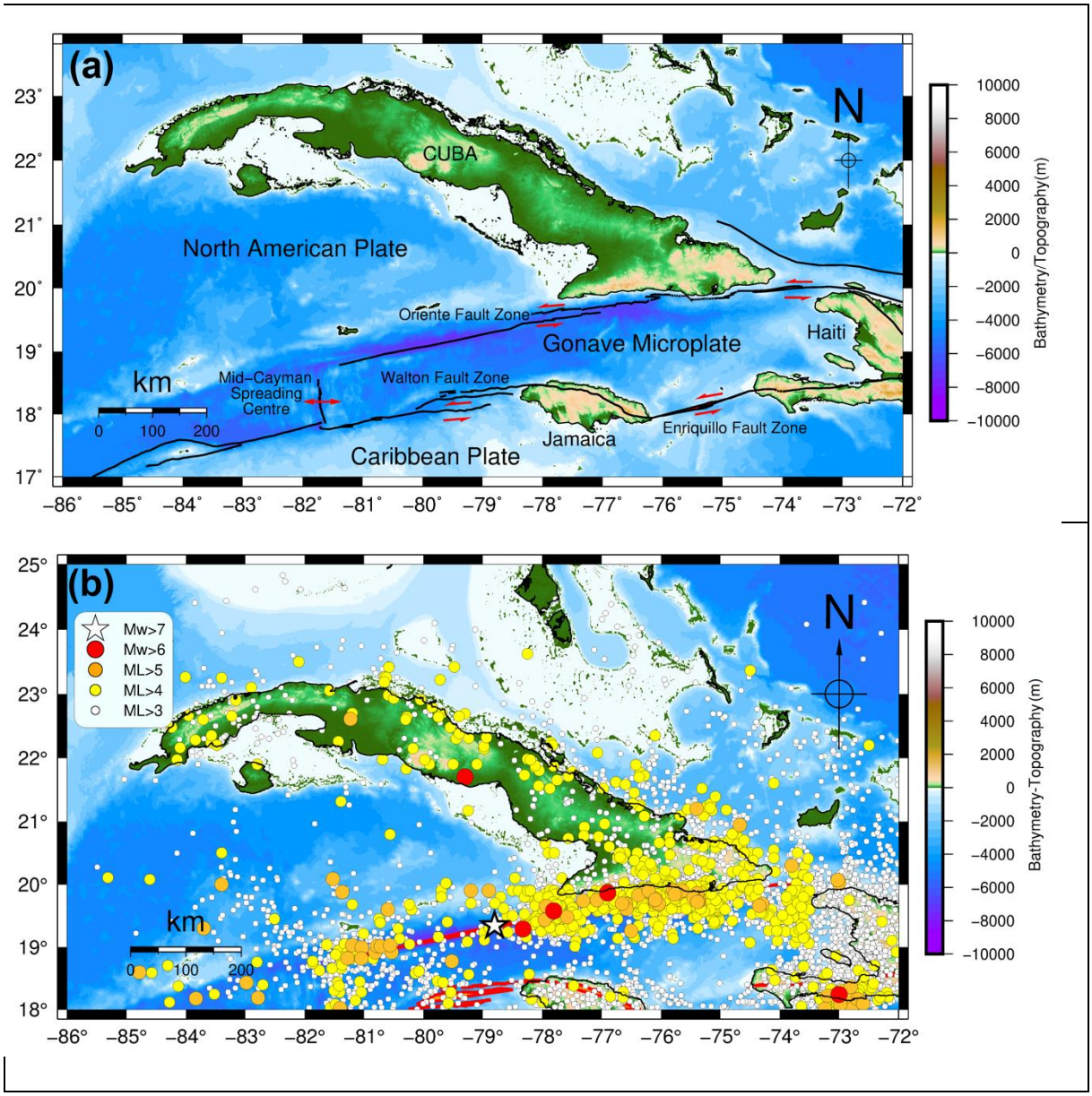
(a)
CUBA
North American Plate
Oriente Fault Zone
Gonave Microplate
Haiti
km
Mid-Cayman Spreading Centre
Walton Fault Zone
0 100 200
Jamaica
Enriquillo Fault Zone
Caribbean Plate
N
Bathymetry/Topography(m)
(b)
Mw>7
Mw>6
ML>5
ML>4
ML>3
Bathymetry-Topography (m)

786 **Figure 1**

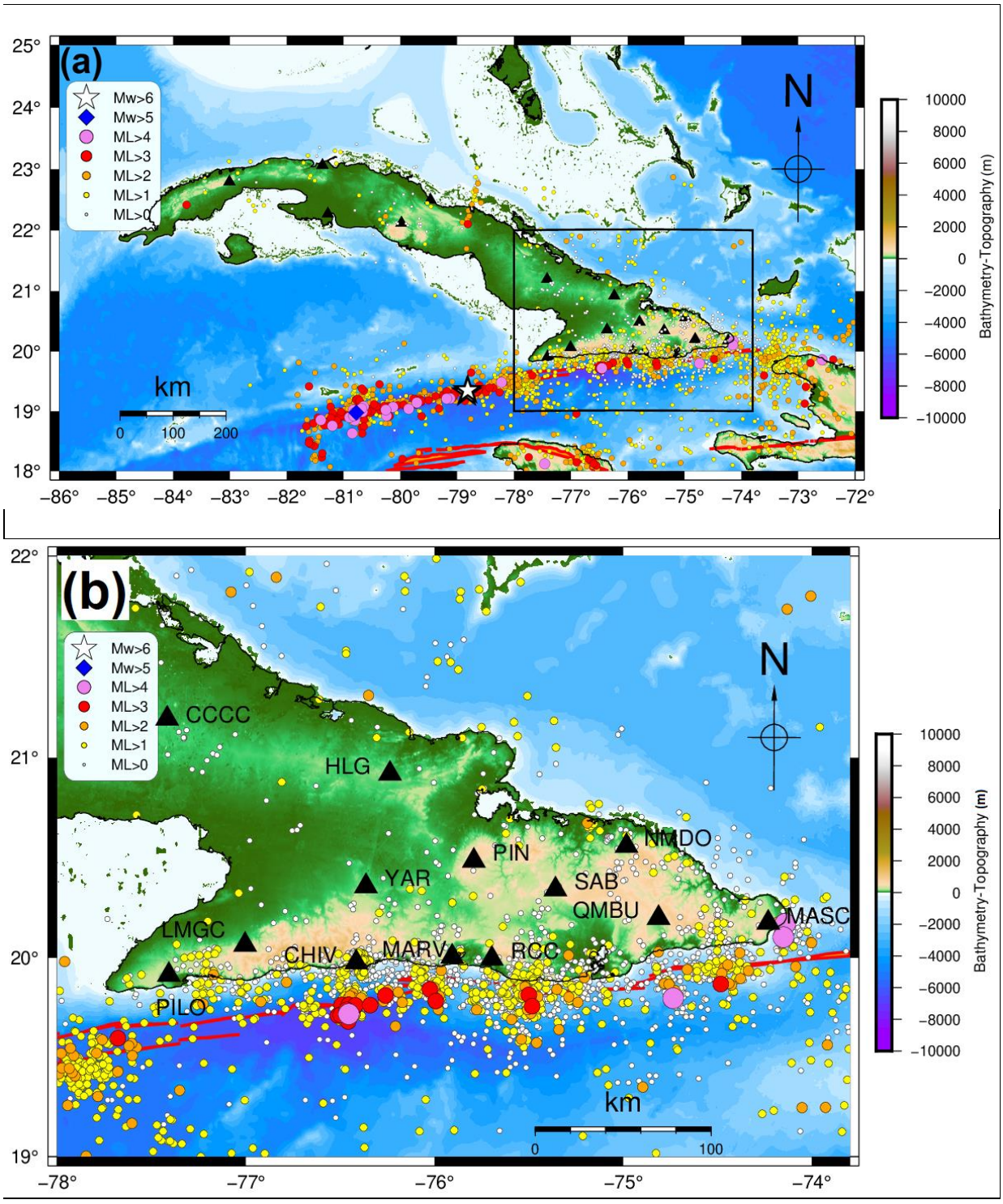
(a)
Mw>6
Mw>5
ML>4
ML>3
ML>2
ML>1
ML>0
N
km
0
100
200
Bathymetry-Topography (m)
10000
8000
6000
4000
2000
0
−2000
−4000
−6000
−8000
−10000
25°
24°
23°
22°
21°
20°
19°
18°
−86°
−85°
−84°
−83°
−82°
−81°
−80°
−79°
−78°
−77°
−76°
−75°
−74°
−73°
−72°
(b)
CCCC
HLG
PIN
NMDO
YAR
SAB
QMBU
MASC
LMGC
CHIV
MARV
RCC
PILO
22°
21°
20°
19°
−78°
−77°
−76°
−75°
−74°

787 **Figure 2**

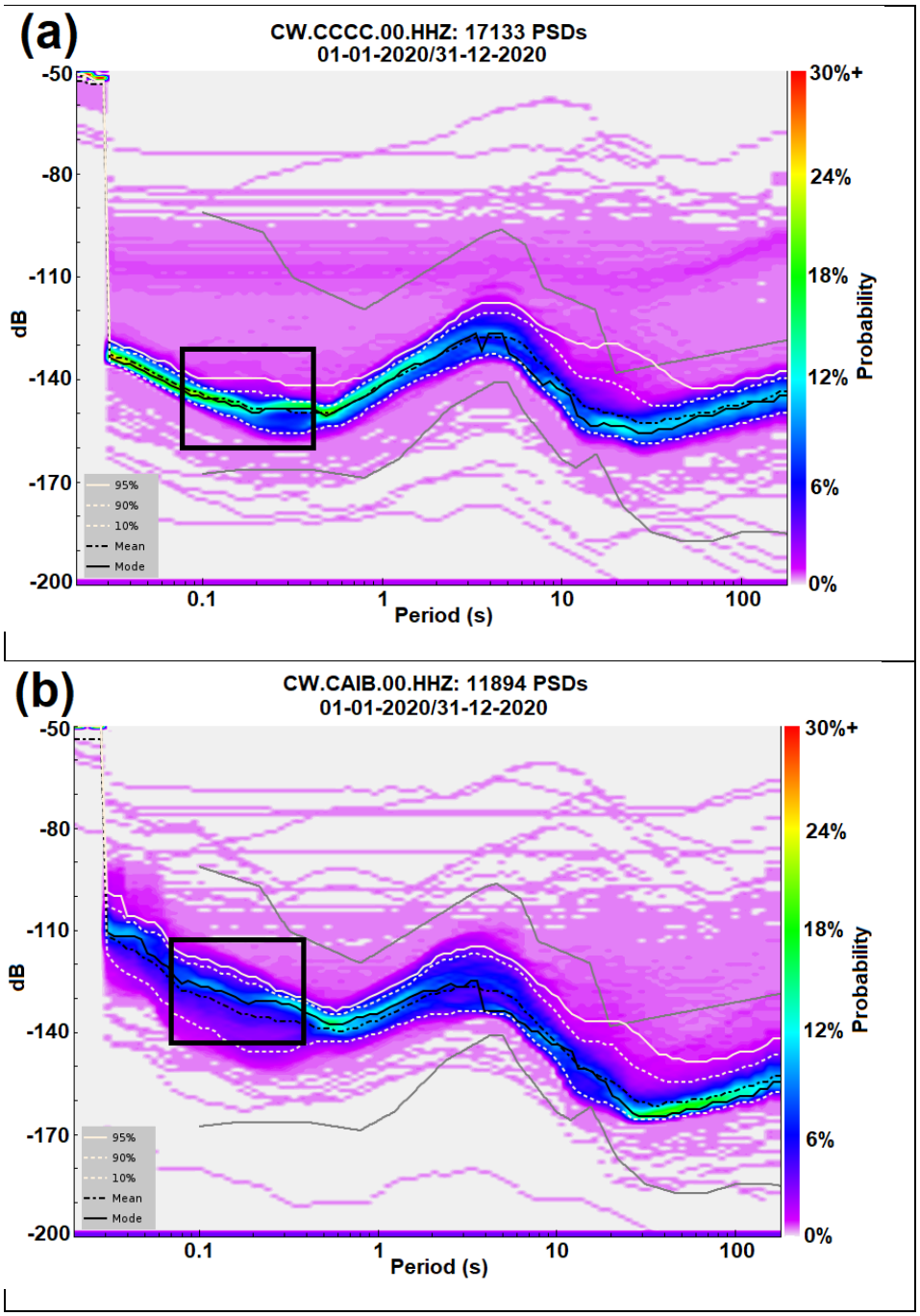
(a)
CW.CCCC.00.HHZ: 17133 PSDs
01-01-2020/31-12-2020
-50
-80
-110
-140
-170
-200
dB
95%
90%
10%
Mean
Mode
0.1
1
10
100
Period (s)
30%+
24%
18%
12%
6%
0%
Probability
(b)
CW.CAIB.00.HHZ: 11894 PSDs
01-01-2020/31-12-2020
-50
-80
-110
-140
-170
-200
dB
95%
90%
10%
Mean
Mode
0.1
1
10
100
Period (s)
30%+
24%
18%
12%
6%
0%
Probability

788 **Figure 3**

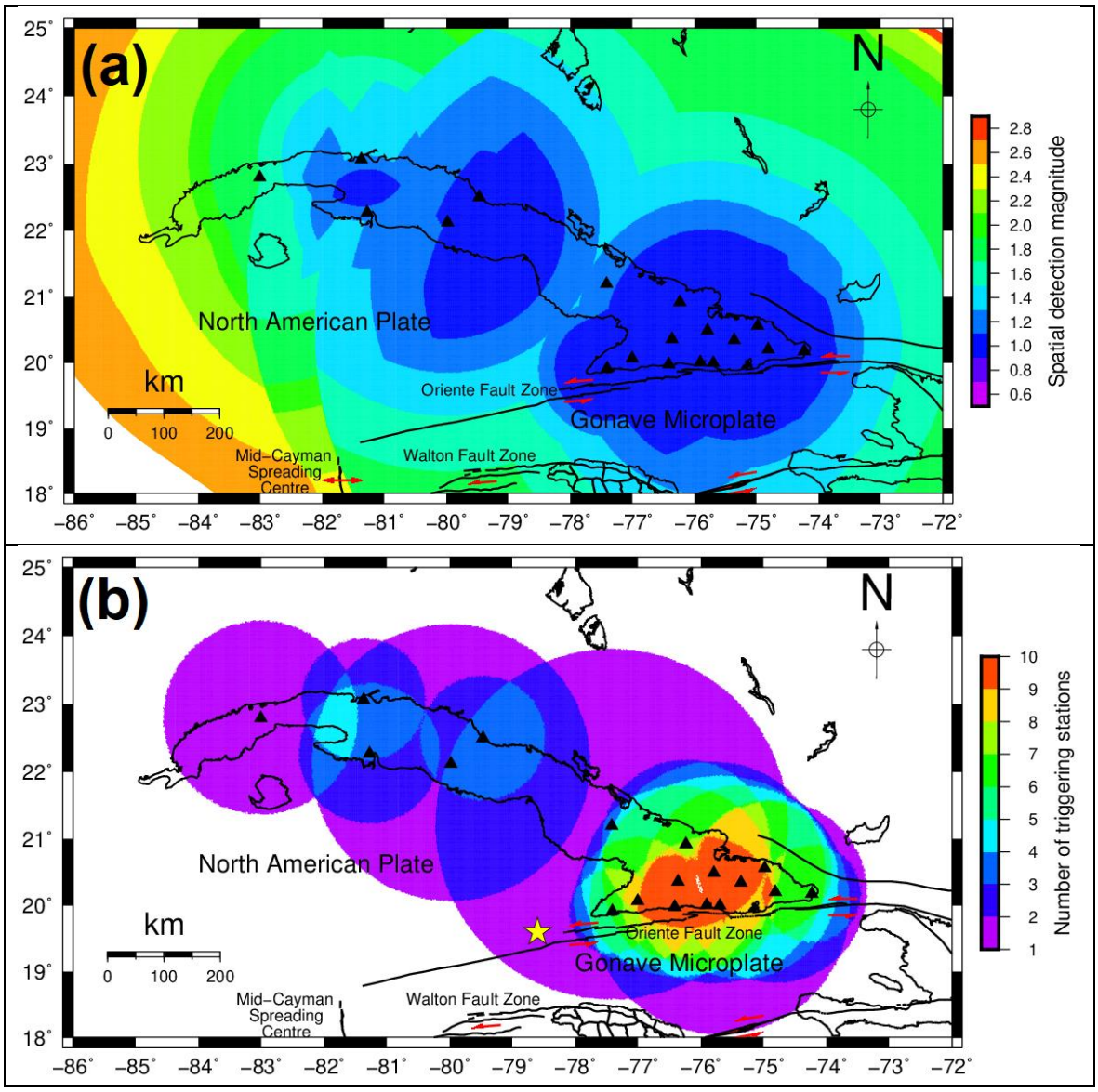

789 **Figure 4**
790

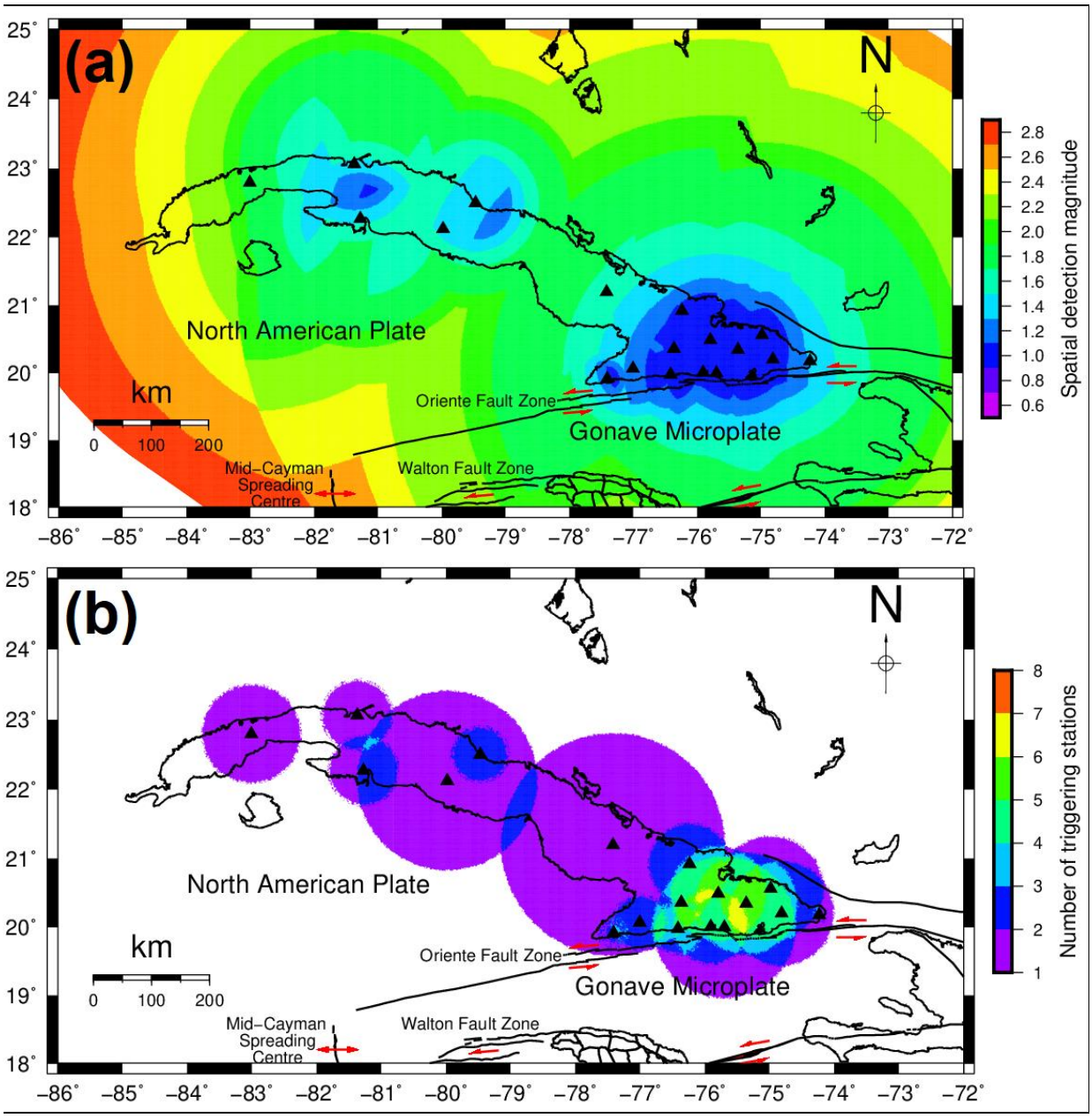
(a)
N
North American Plate
km
0 100 200
Oriente Fault Zone
Gonave Microplate
Mid–Cayman Spreading Centre
Walton Fault Zone
Spatial detection magnitude
2.8
2.6
2.4
2.2
2.0
1.8
1.6
1.4
1.2
1.0
0.8
0.6
(b)
N
North American Plate
km
0 100 200
Oriente Fault Zone
Gonave Microplate
Mid–Cayman Spreading Centre
Walton Fault Zone
Number of triggering stations
8
7
6
5
4
3
2
1
25˚
24˚
23˚
22˚
21˚
20˚
19˚
18˚
–86˚ –85˚ –84˚ –83˚ –82˚ –81˚ –80˚ –79˚ –78˚ –77˚ –76˚ –75˚ –74˚ –73˚ –72˚

Figure 5

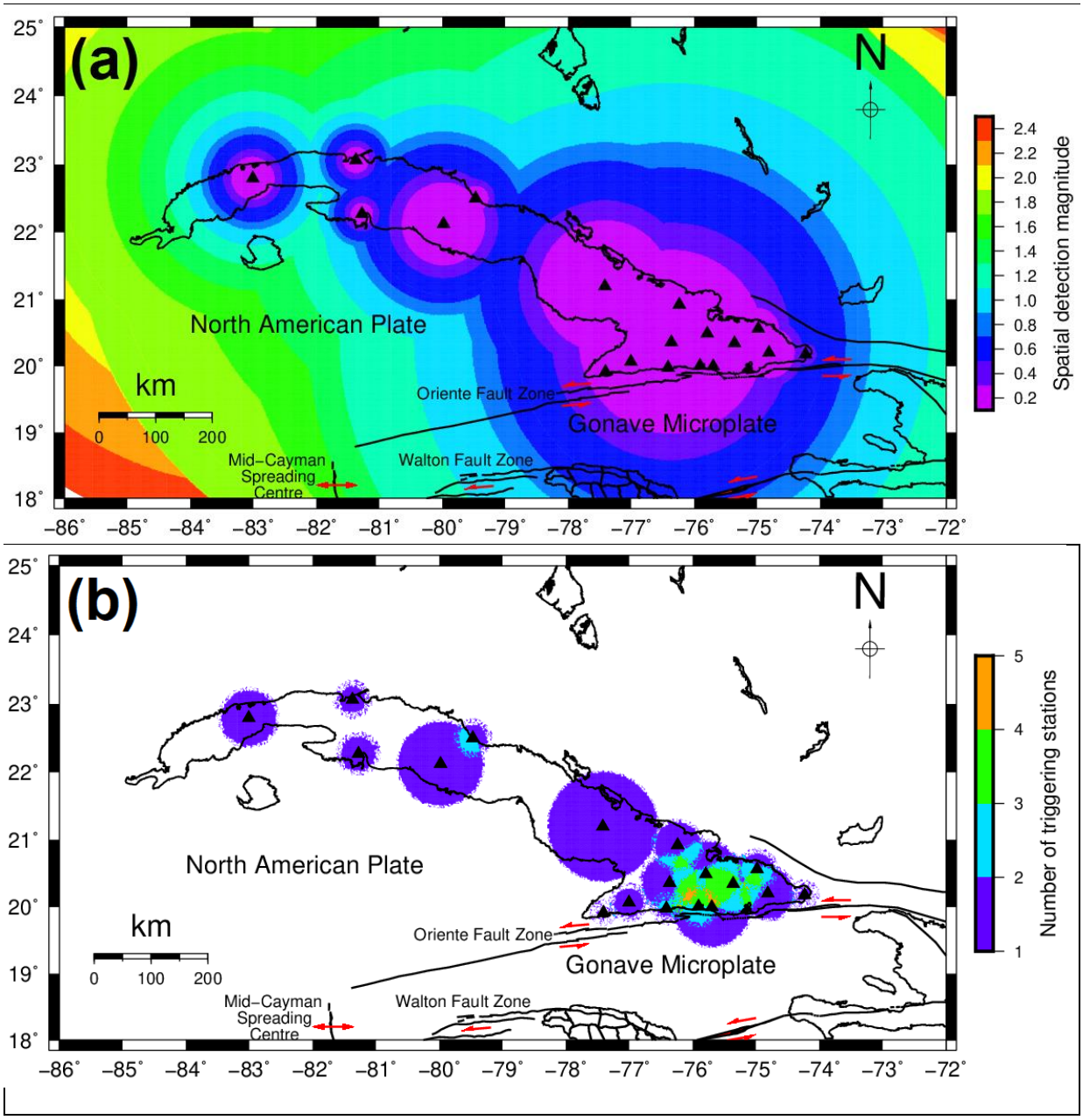
(a)
N
North American Plate
km
0 100 200
Oriente Fault Zone
Gonave Microplate
Mid–Cayman Spreading Centre
Walton Fault Zone
Spatial detection magnitude
2.4
2.2
2.0
1.8
1.6
1.4
1.2
1.0
0.8
0.6
0.4
0.2
(b)
N
North American Plate
km
0 100 200
Oriente Fault Zone
Gonave Microplate
Mid–Cayman Spreading Centre
Walton Fault Zone
Number of triggering stations
5
4
3
2
1
25°
24°
23°
22°
21°
20°
19°
18°
–86° –85° –84° –83° –82° –81° –80° –79° –78° –77° –76° –75° –74° –73° –72°

793 **Figure 6**

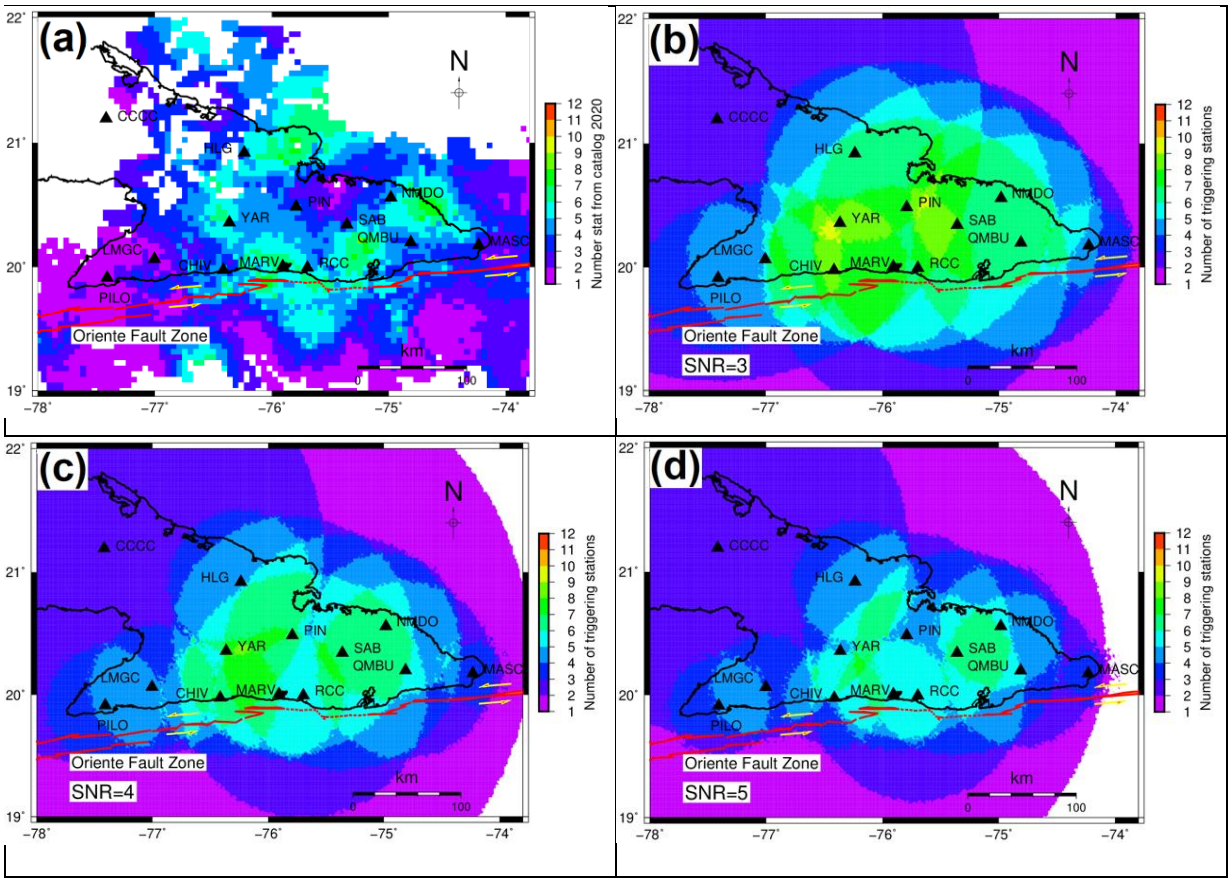

794 **Figure 7**

795

APPENDIX A

We have extracted from the earthquake catalog Cuban National Seismological Centre a selection corresponding to the earthquakes occurred in the year 2020. This catalog has been used for validating the results of the theoretical estimations of the detection capability of the Cuban seismic network. The 2020 earthquake catalog reports all earthquakes detected and localized in the region surrounding the Cuba island. The catalog uses data not only of the Cuban seismic network, but also of other stations of the Caribbean region, and it also reports recognized by manual inspection, in some cases triggered by 1 station.

Figure A1 shows the maps of the 2020 catalog for the whole Cuban territory (panel a) and of the events with $0.9 \leq M_L \leq 1.1$ localized in the eastern part of the island, respectively. (panels a and b, respectively). For each event, the color corresponds to the number of the triggered stations.

The Cuban 2020 earthquake catalog is delivered as an Electronic Supplement to this paper as **Data Set DS01.**

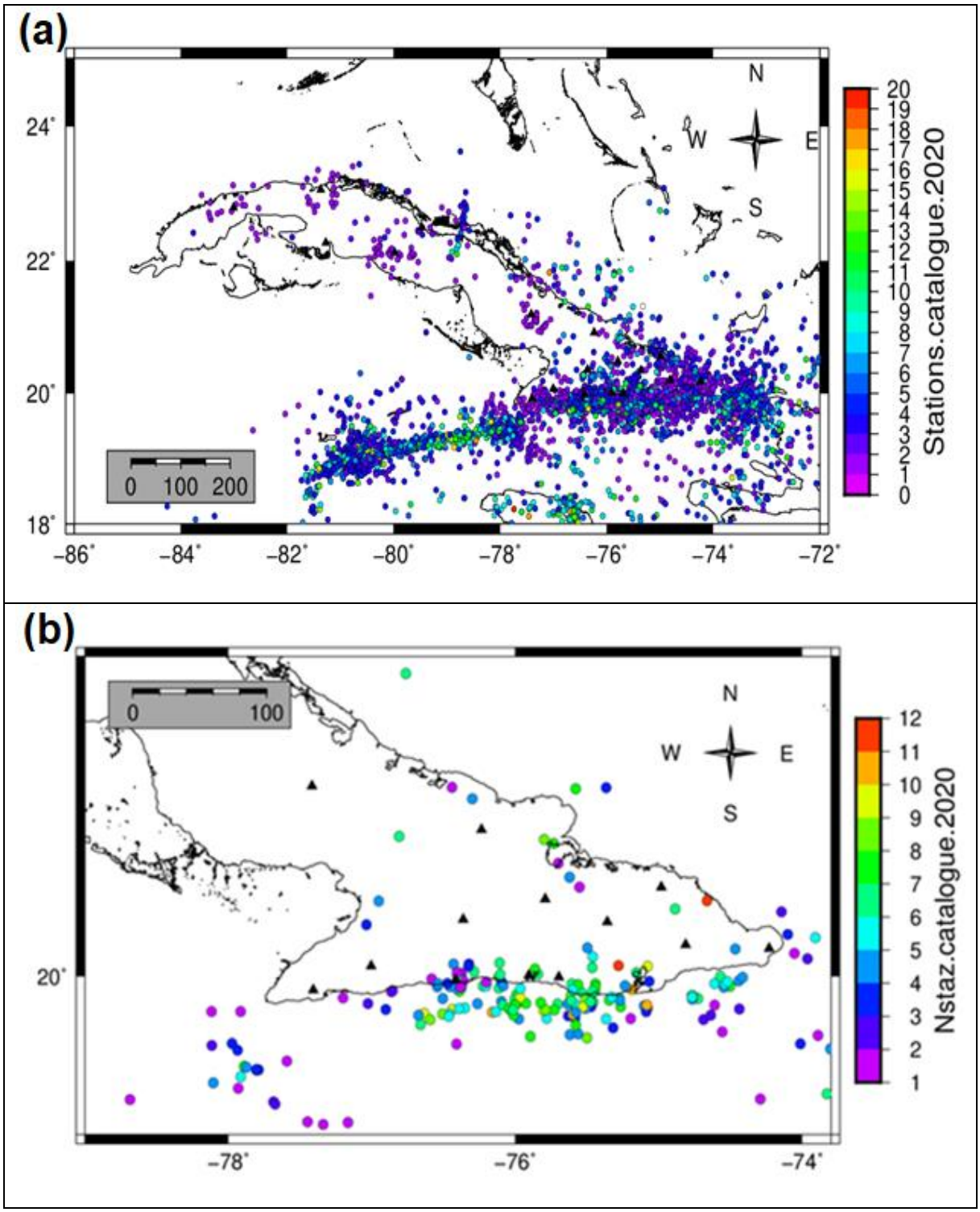
(a)
24°
22°
20°
18°
−86°
−84°
−82°
−80°
−78°
−76°
−74°
−72°
N
W
E
S
0 100 200
Stations.catalogue.2020
20
19
18
17
16
15
14
13
12
11
10
9
8
7
6
5
4
3
2
1
0
(b)
0 100
N
W
E
S
20°
−78°
−76°
−74°
Nstaz.catalogue.2020
12
11
10
9
8
7
6
5
4
3
2
1

Figure A1

Figure 1b

Click here to access/download;Figure;Figura_1b.jpg

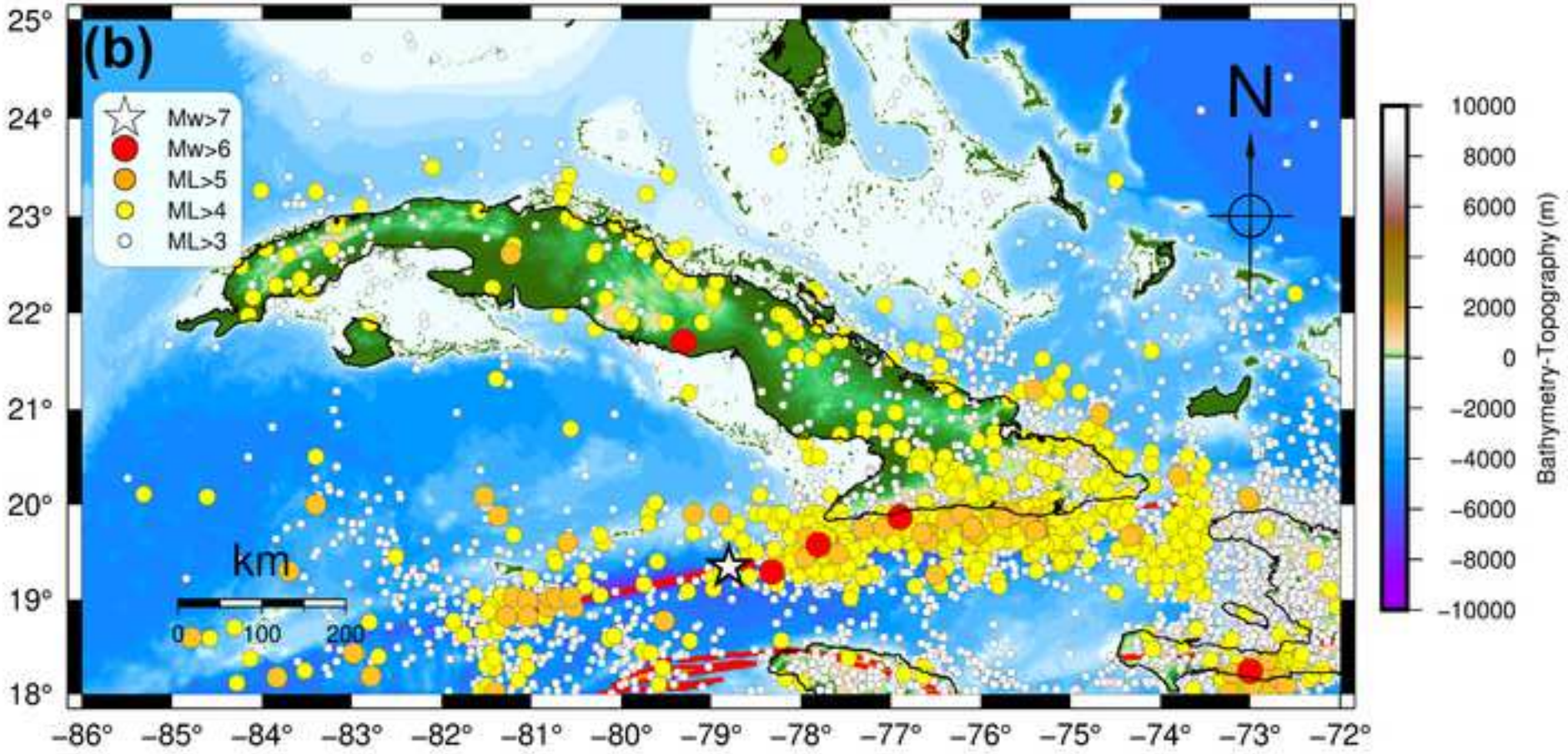

Figure 2a

Click here to access/download;Figure;Figura_2a.jpg

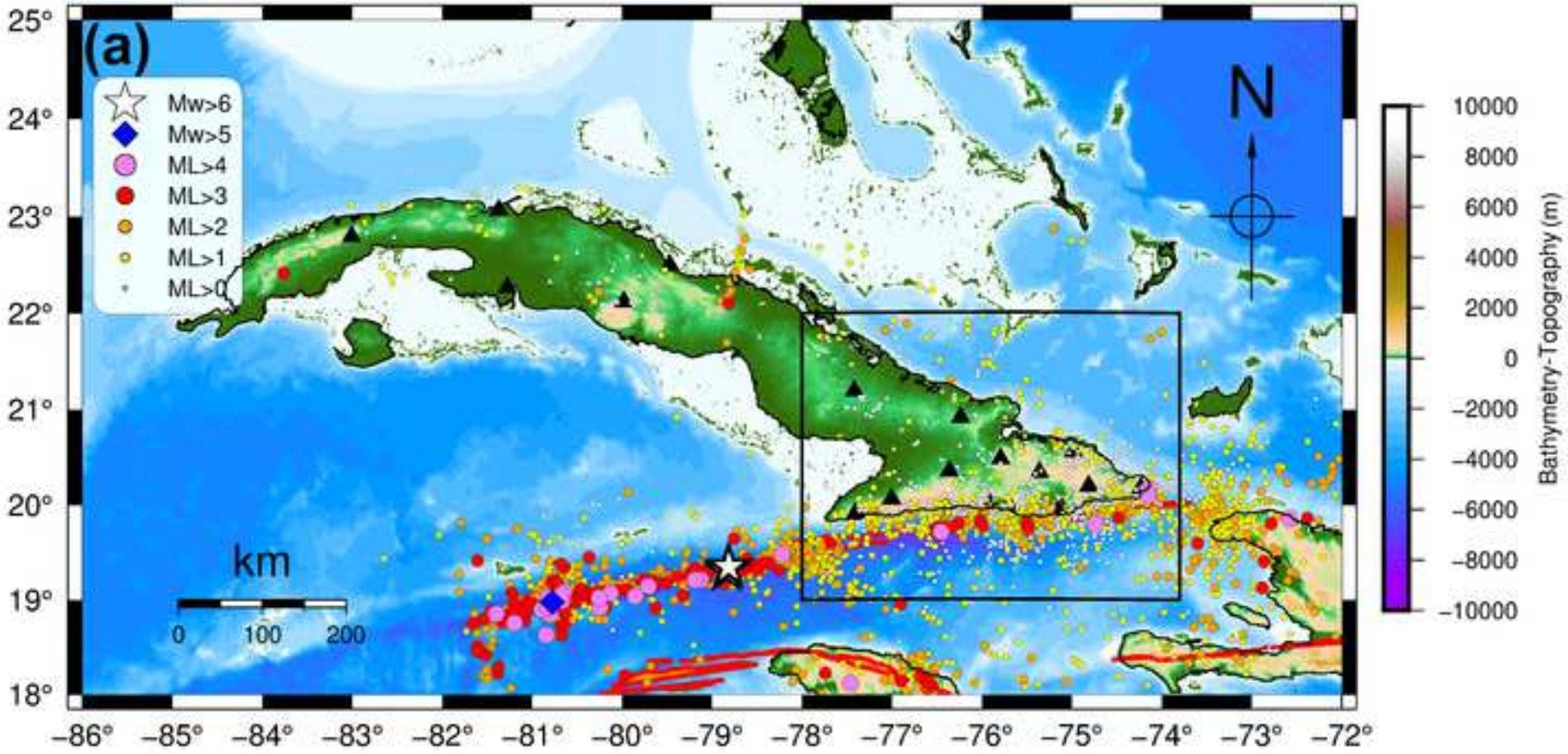

Figure 2b

Click here to access/download;Figure;Figura_2b.jpg

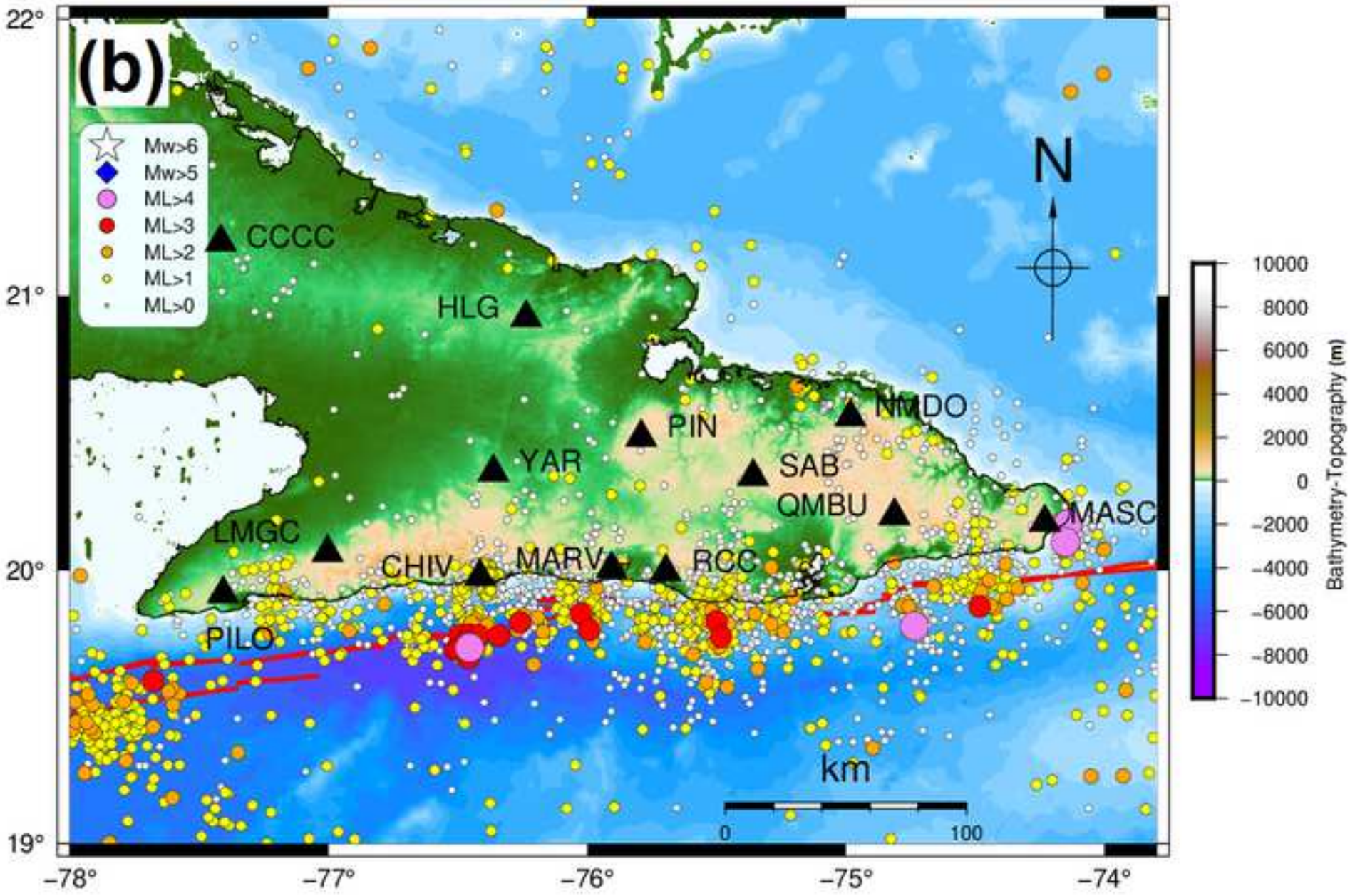

Figure 3a

Click here to access/download;Figure;Figura_3a.jpg

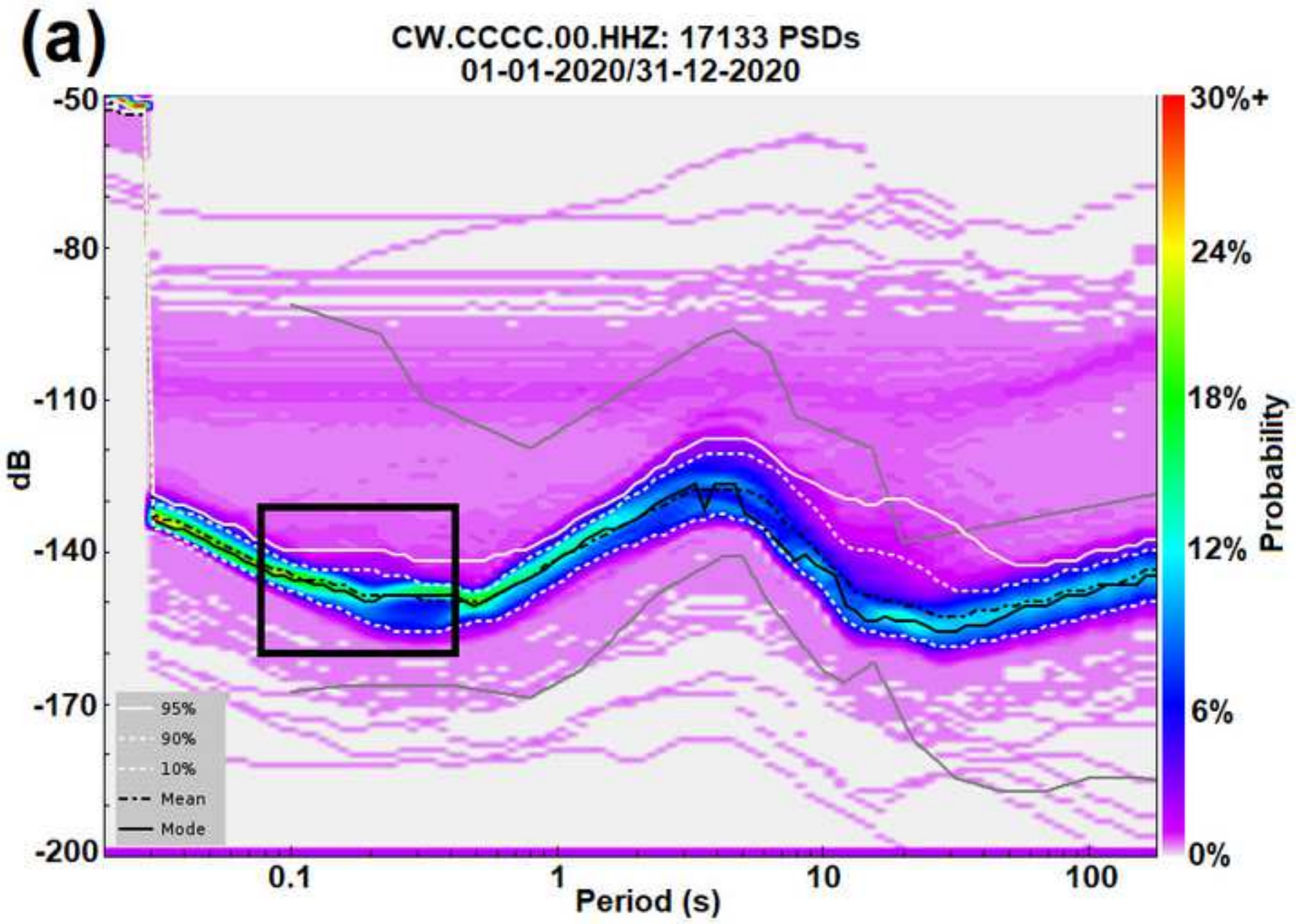

Figure 3b

Click here to access/download;Figure;Figura_3b.jpg

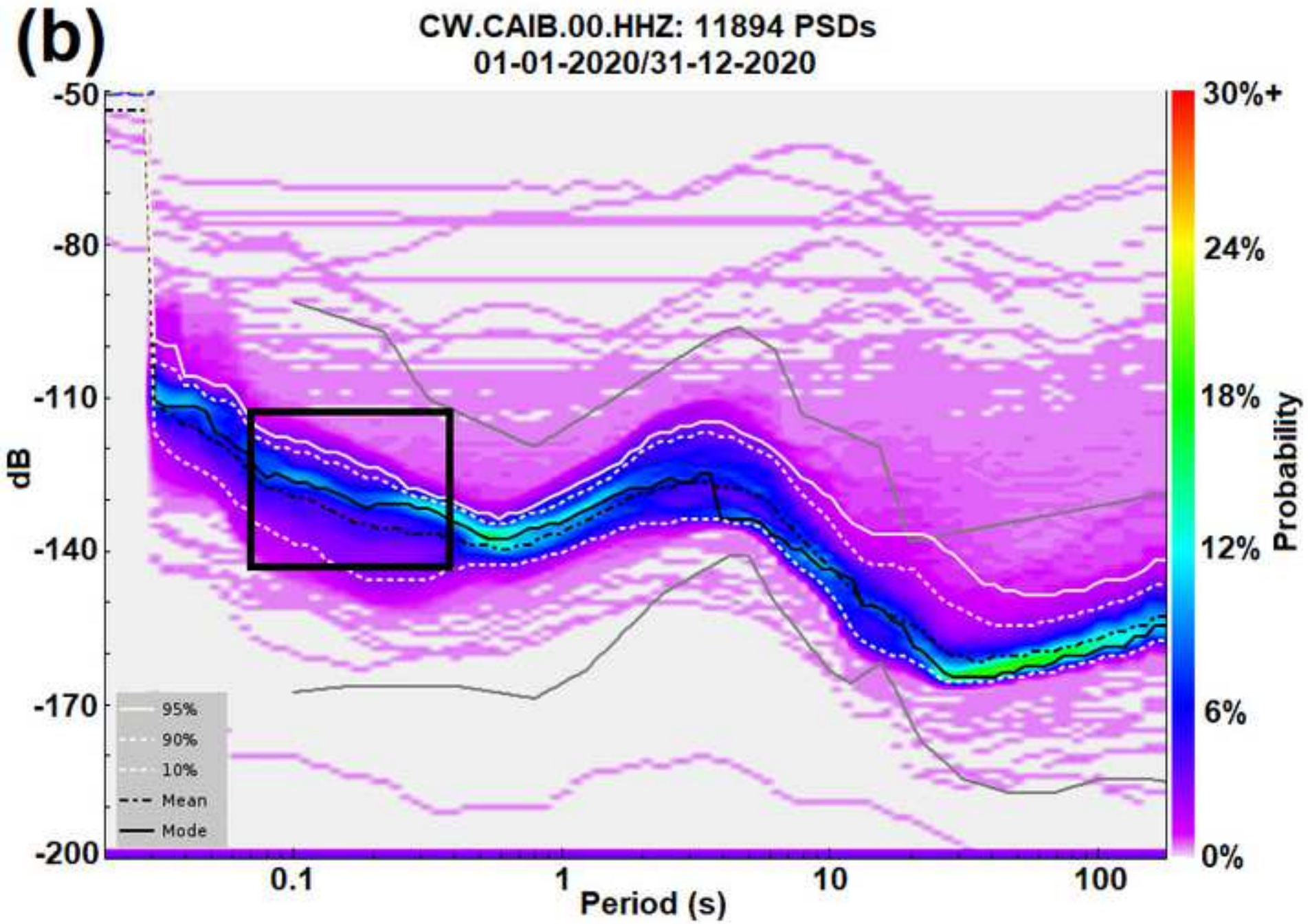

Figure 4a

Click here to access/download;Figure;Figura_4a.jpg

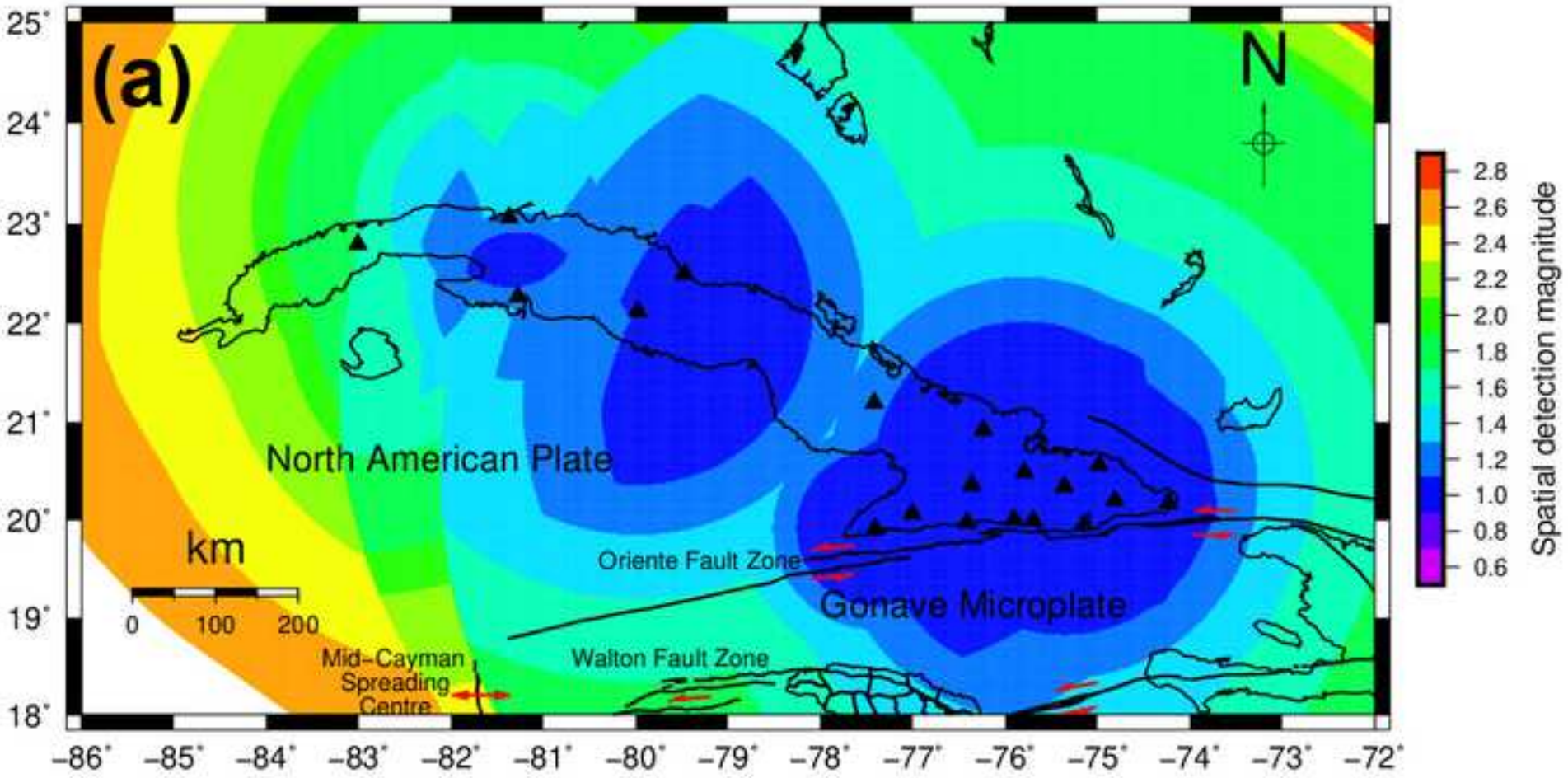

Figure 4b

Click here to access/download;Figure;Figura_4b.jpg

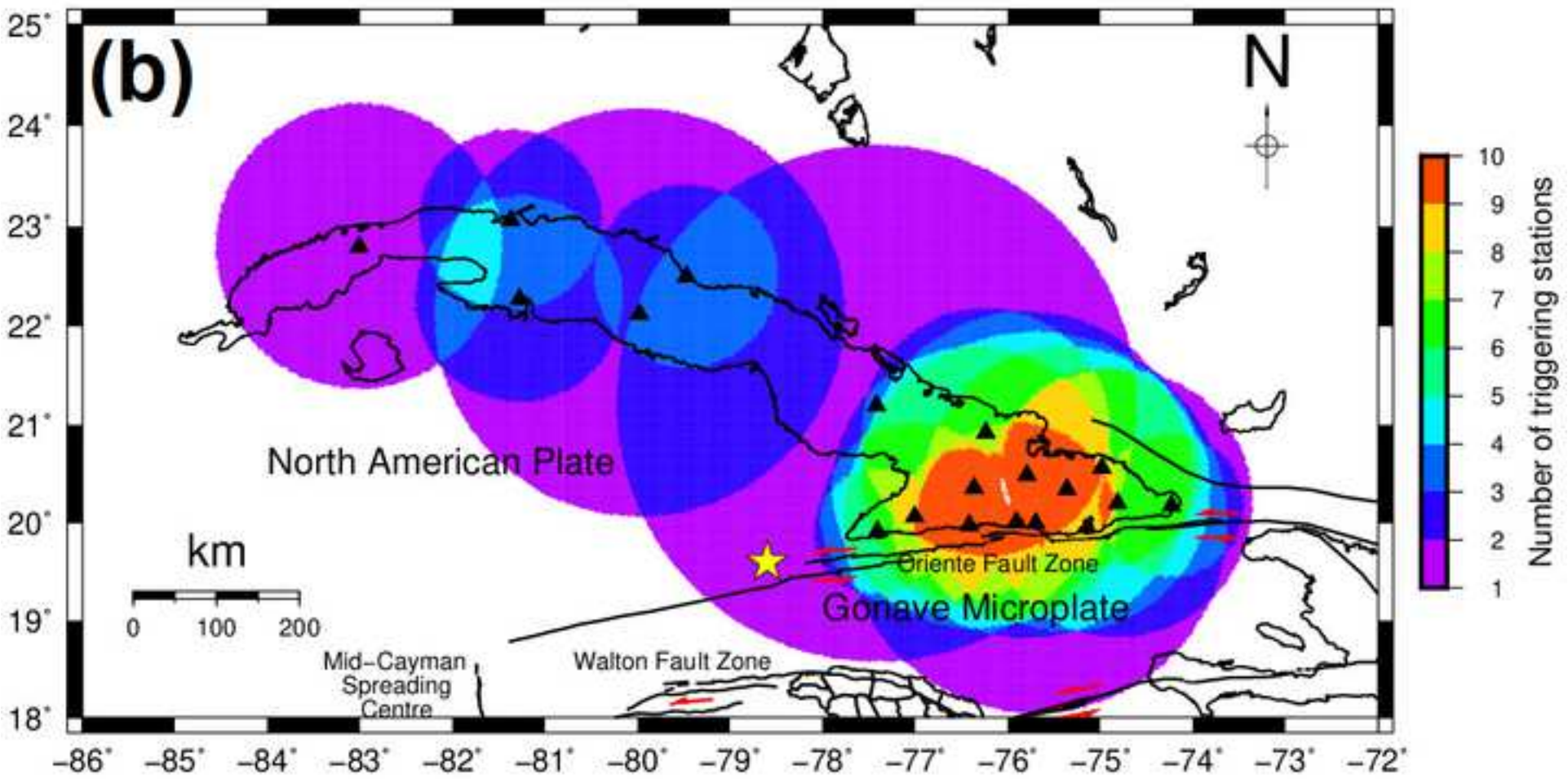

Figure 5a

Click here to access/download;Figure;Figura_5a.jpg

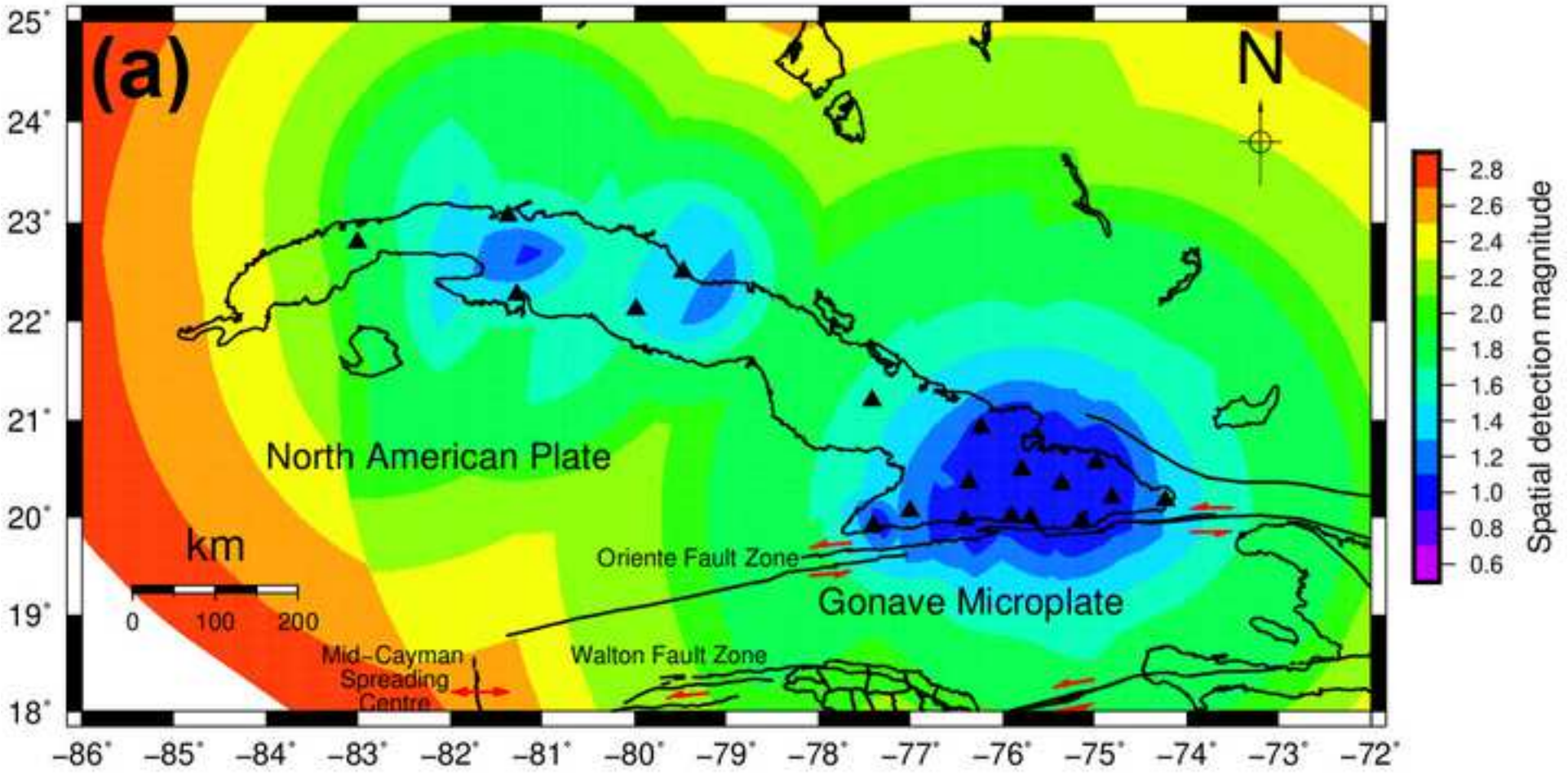

Figure 5b

Click here to access/download;Figure;Figura_5b.jpg

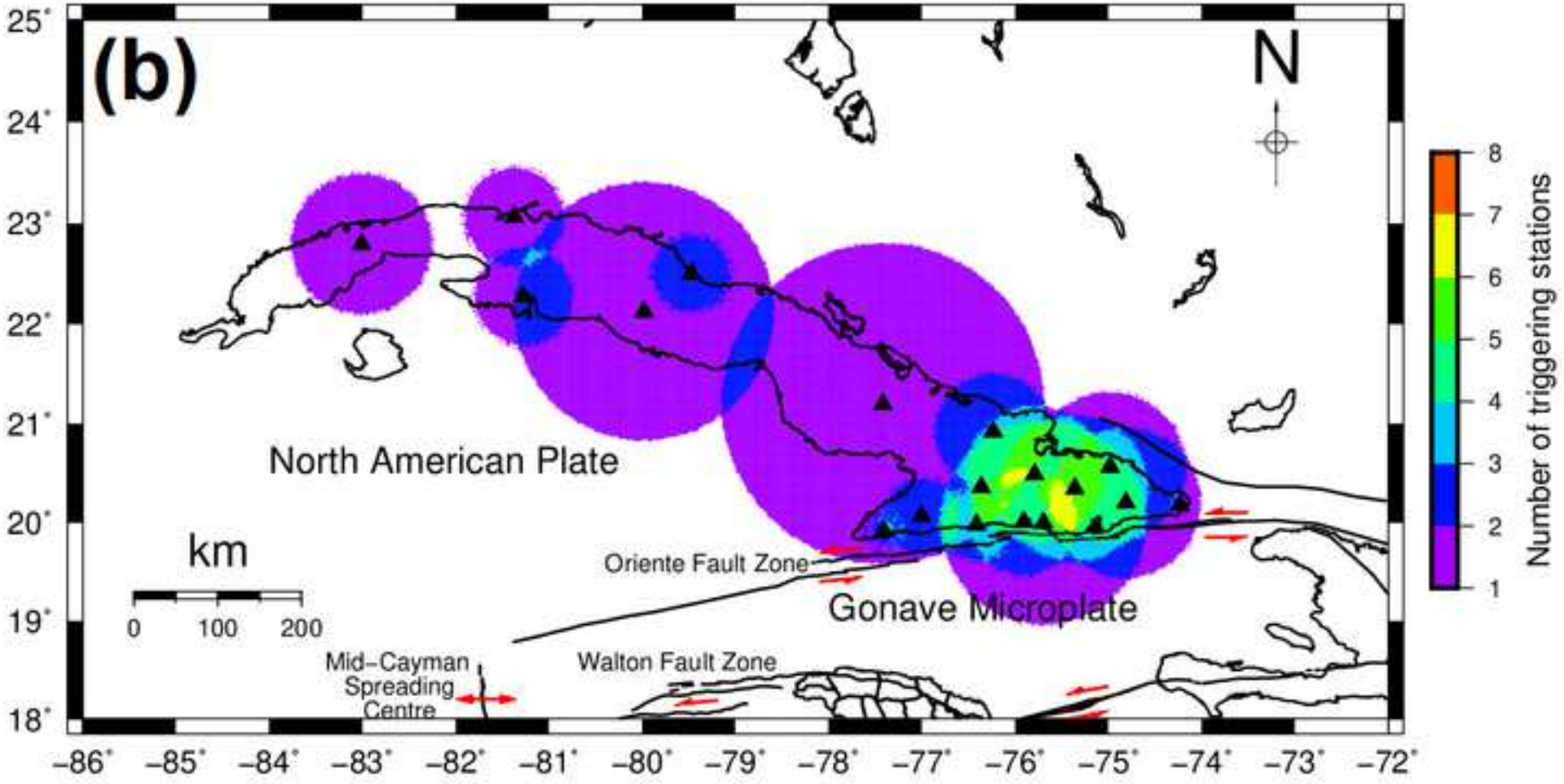

Figure 6a

Click here to access/download;Figure;Figura_6a.jpg

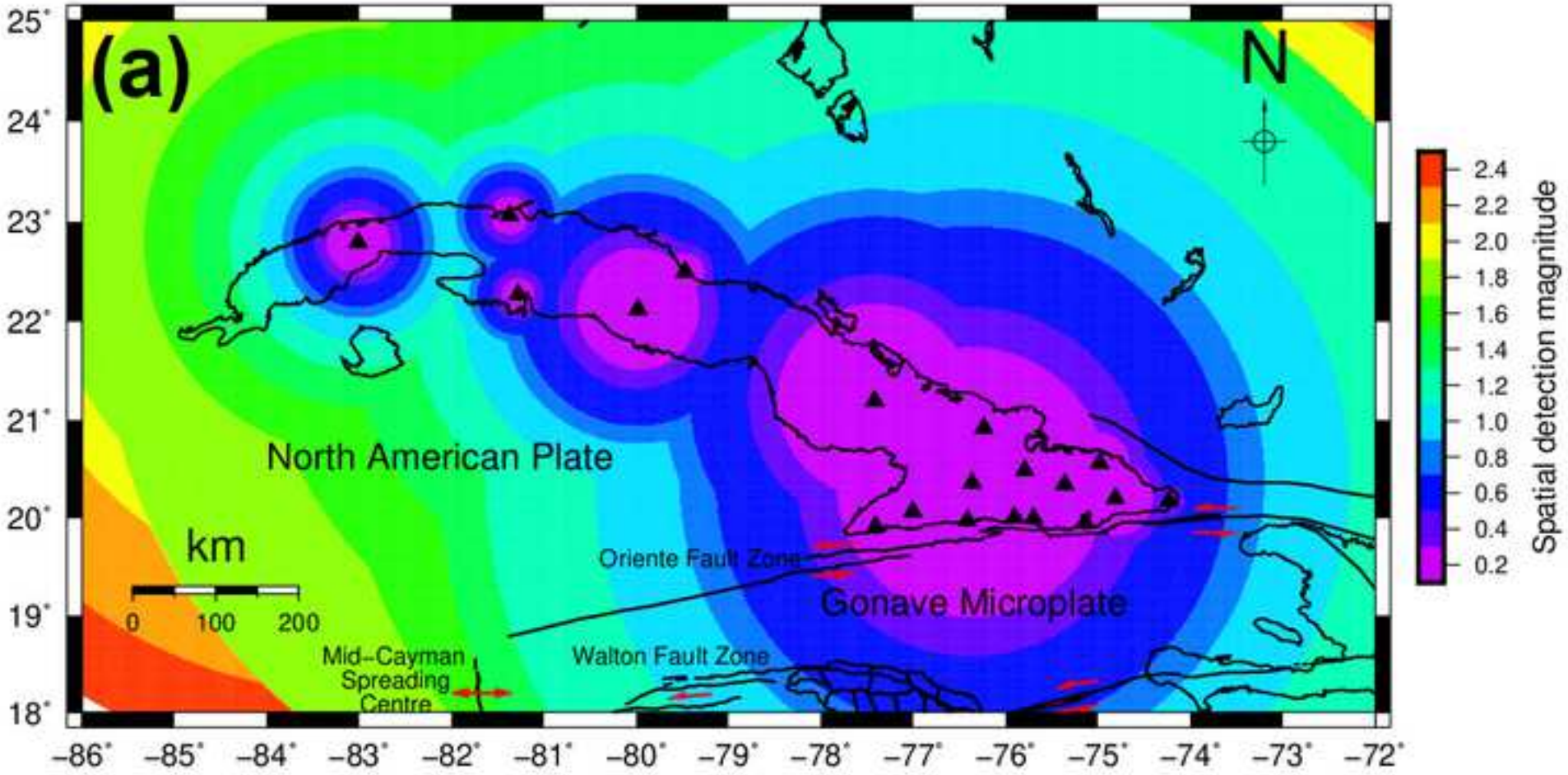

Figure 6b

Click here to access/download;Figure;Figura_6b.jpg

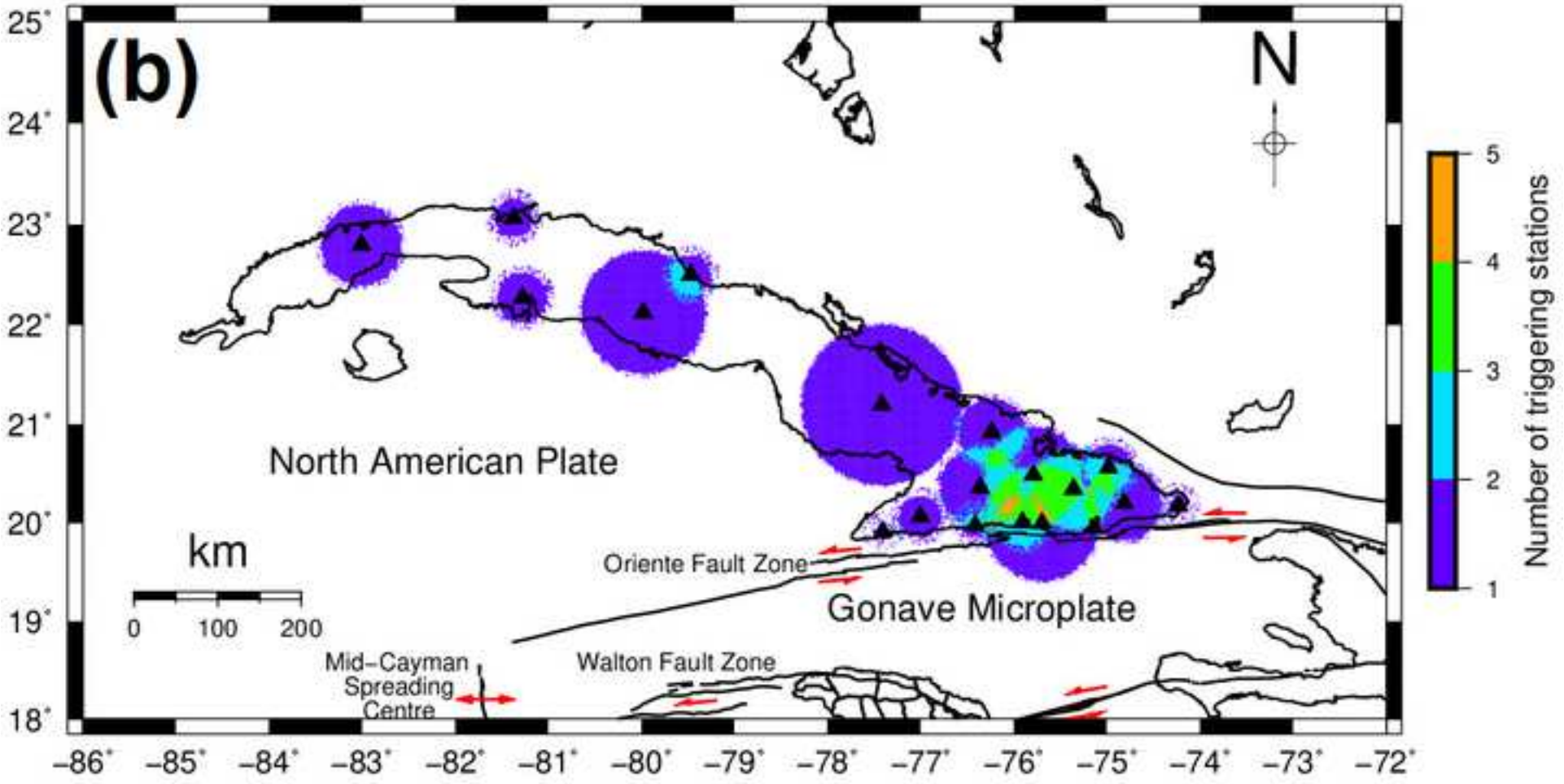

Figure 7a

Click here to access/download;Figure;Figura_7a.jpg

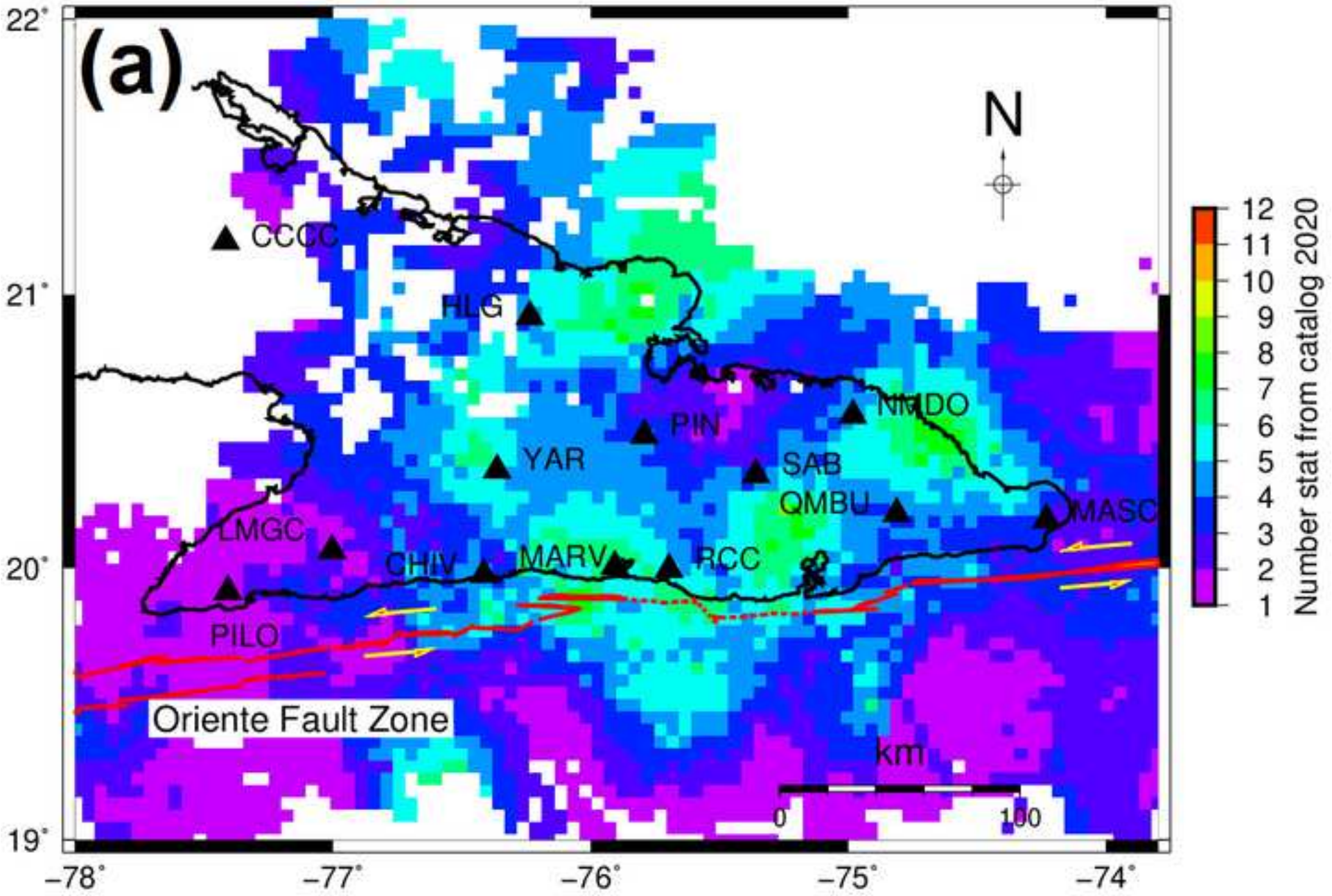

Figure 7b

Click here to access/download;Figure;Figura_7b.jpg

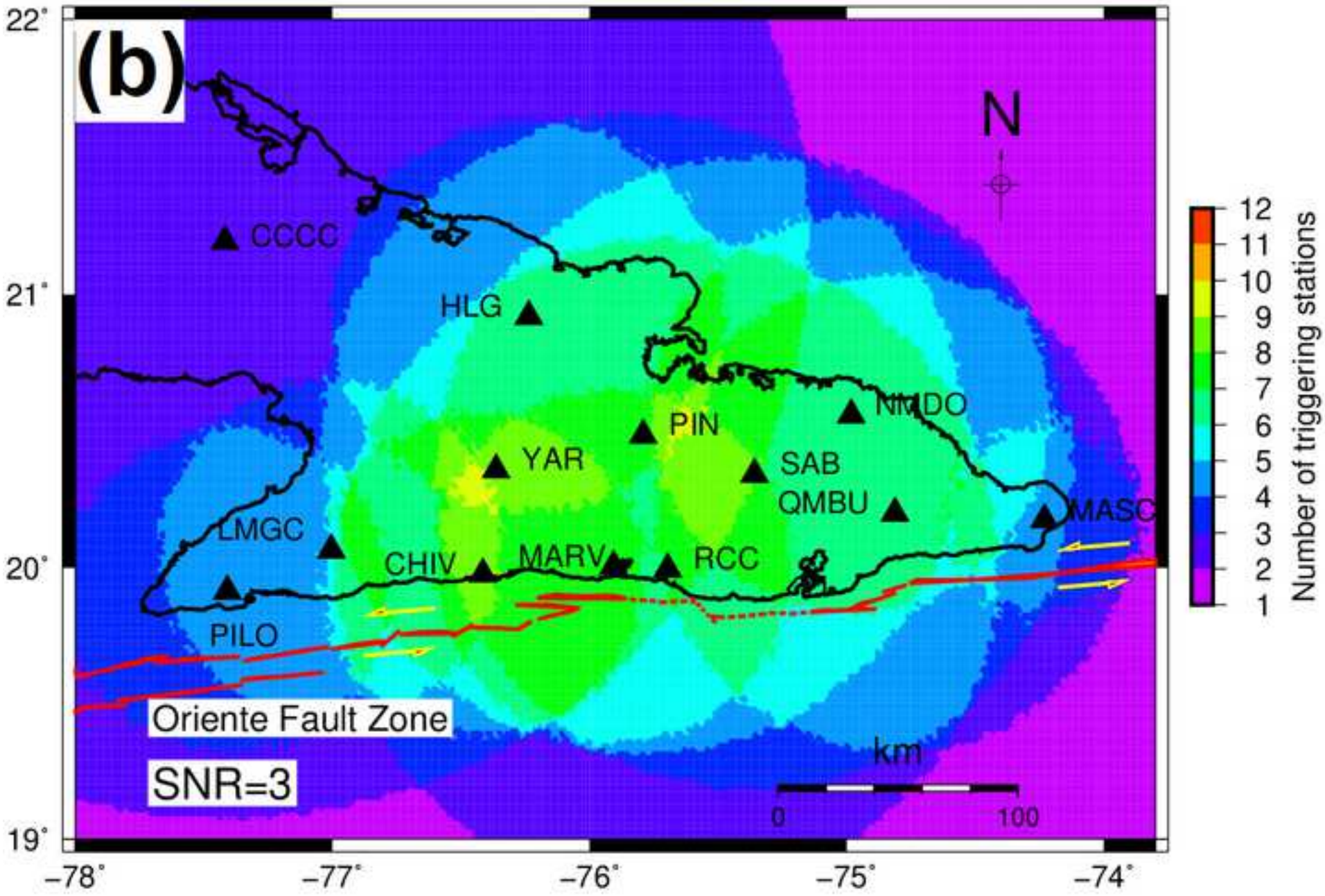

Figure 7c

Click here to access/download;Figure;Figura_7c.jpg

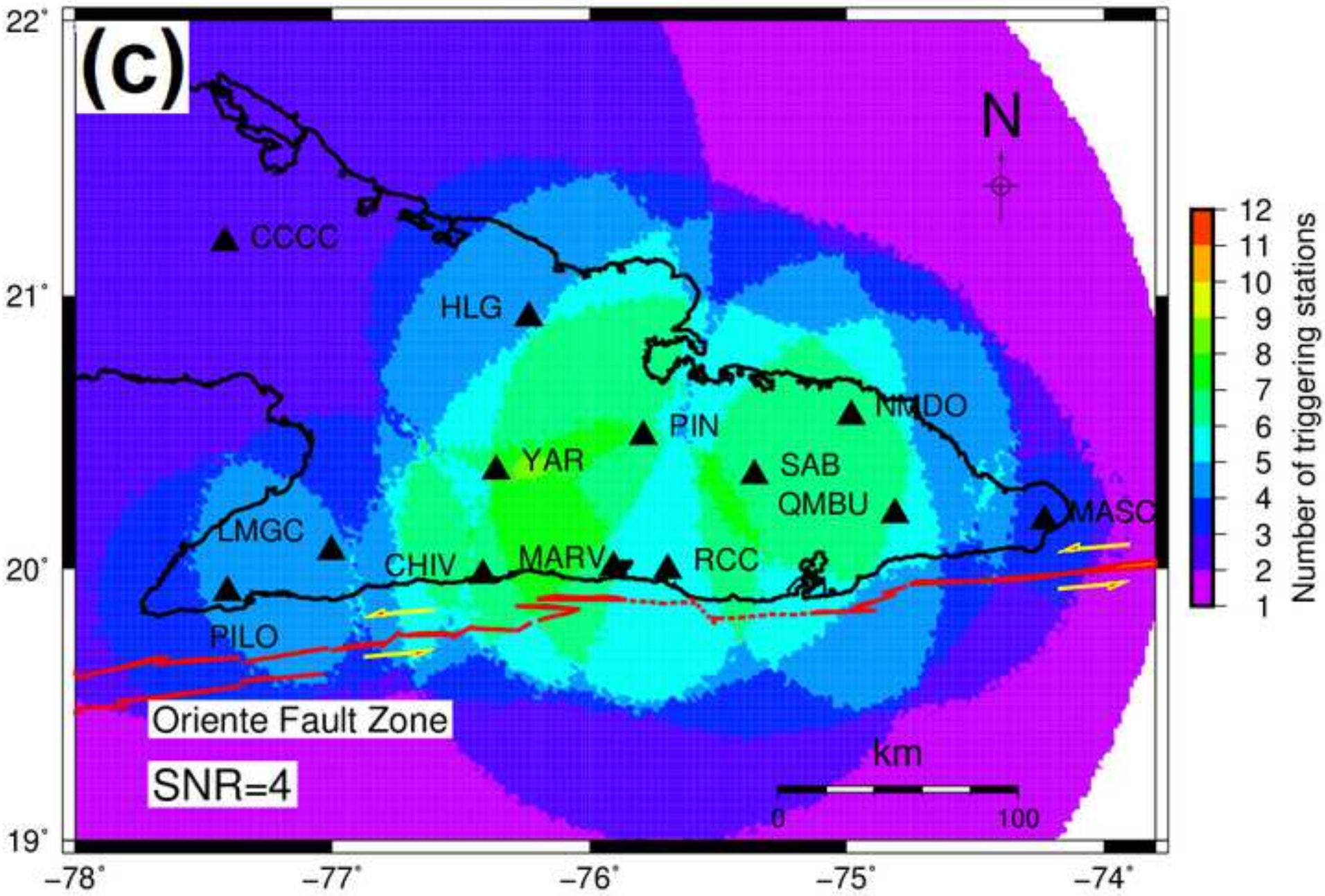

Figure 7d

Click here to access/download;Figure;Figura_7d.jpg

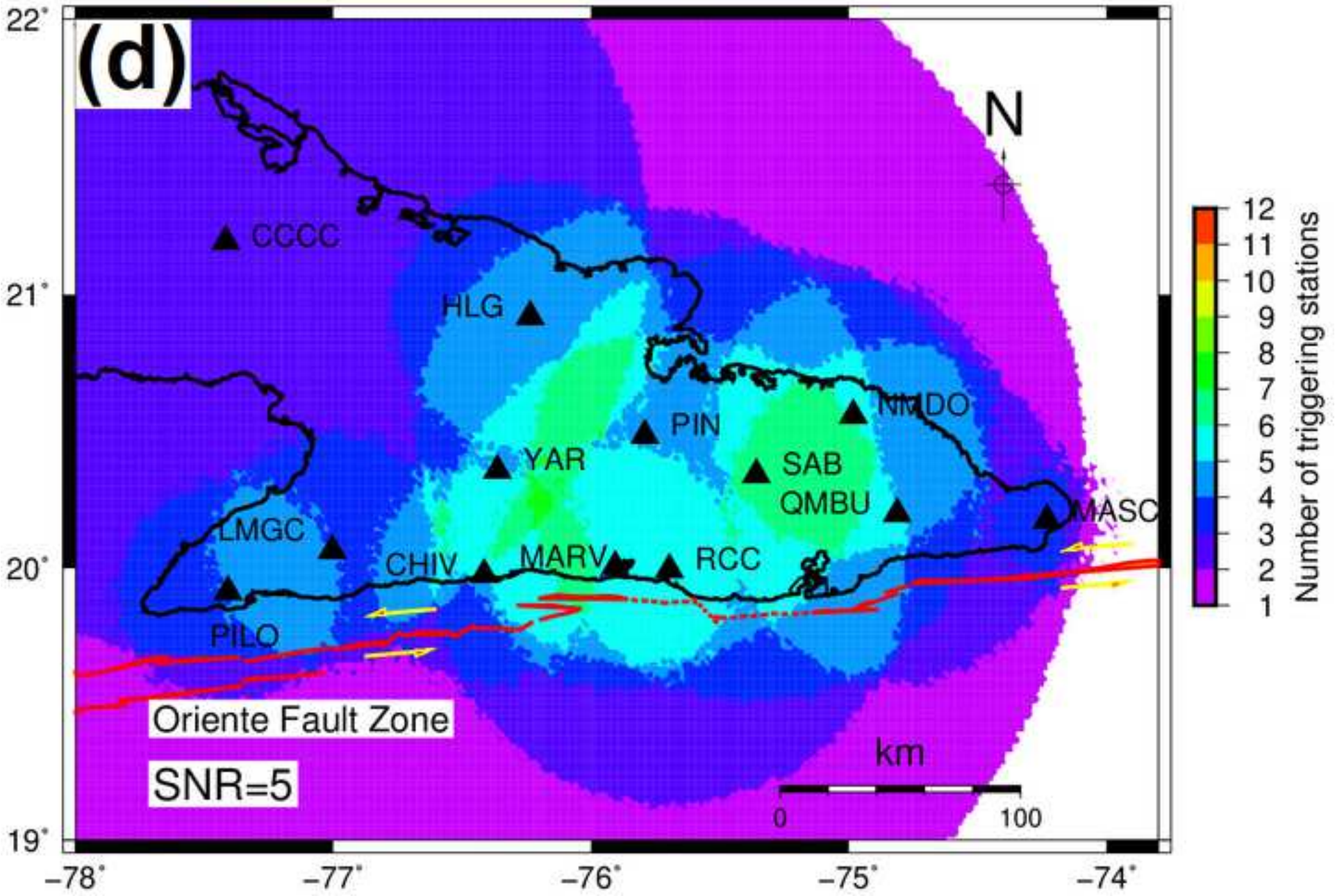

Figure 1a

Click here to access/download;Figure;Figura_1a.jpg

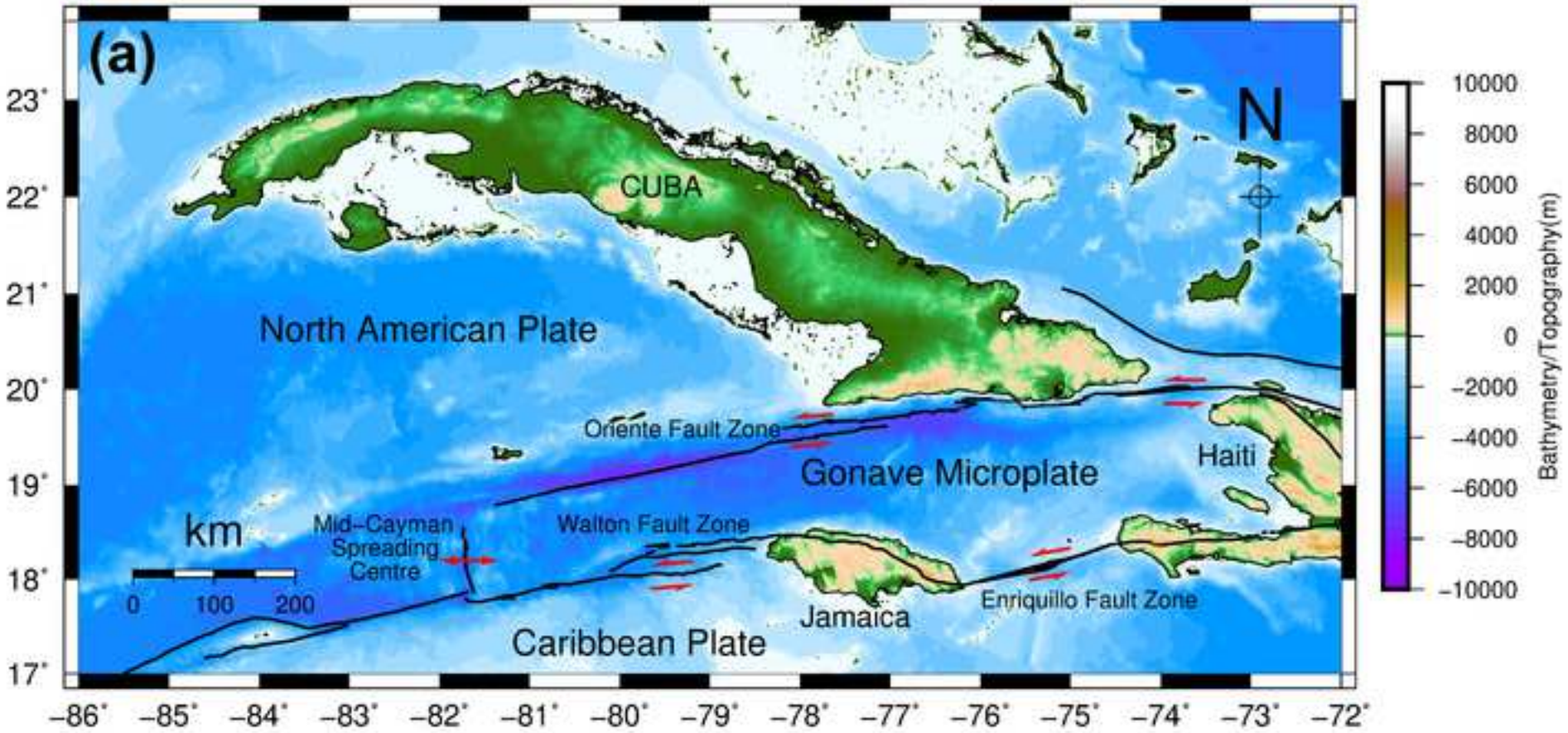

Figure A1a

Click here to access/download;Figure;Figura_A1a.jpg

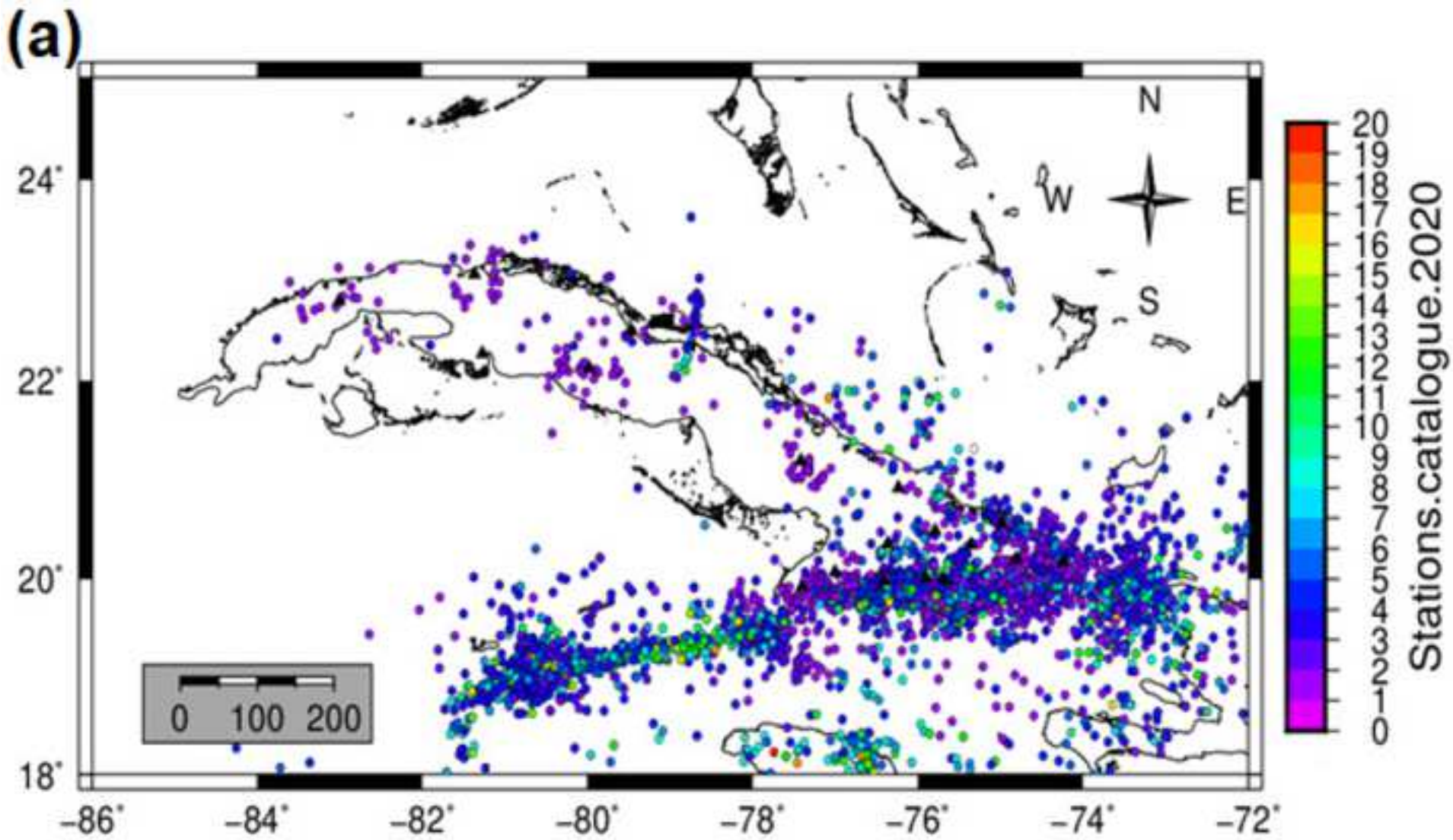

Figure A1b

Click here to access/download;Figure;Figura_A1b.jpg

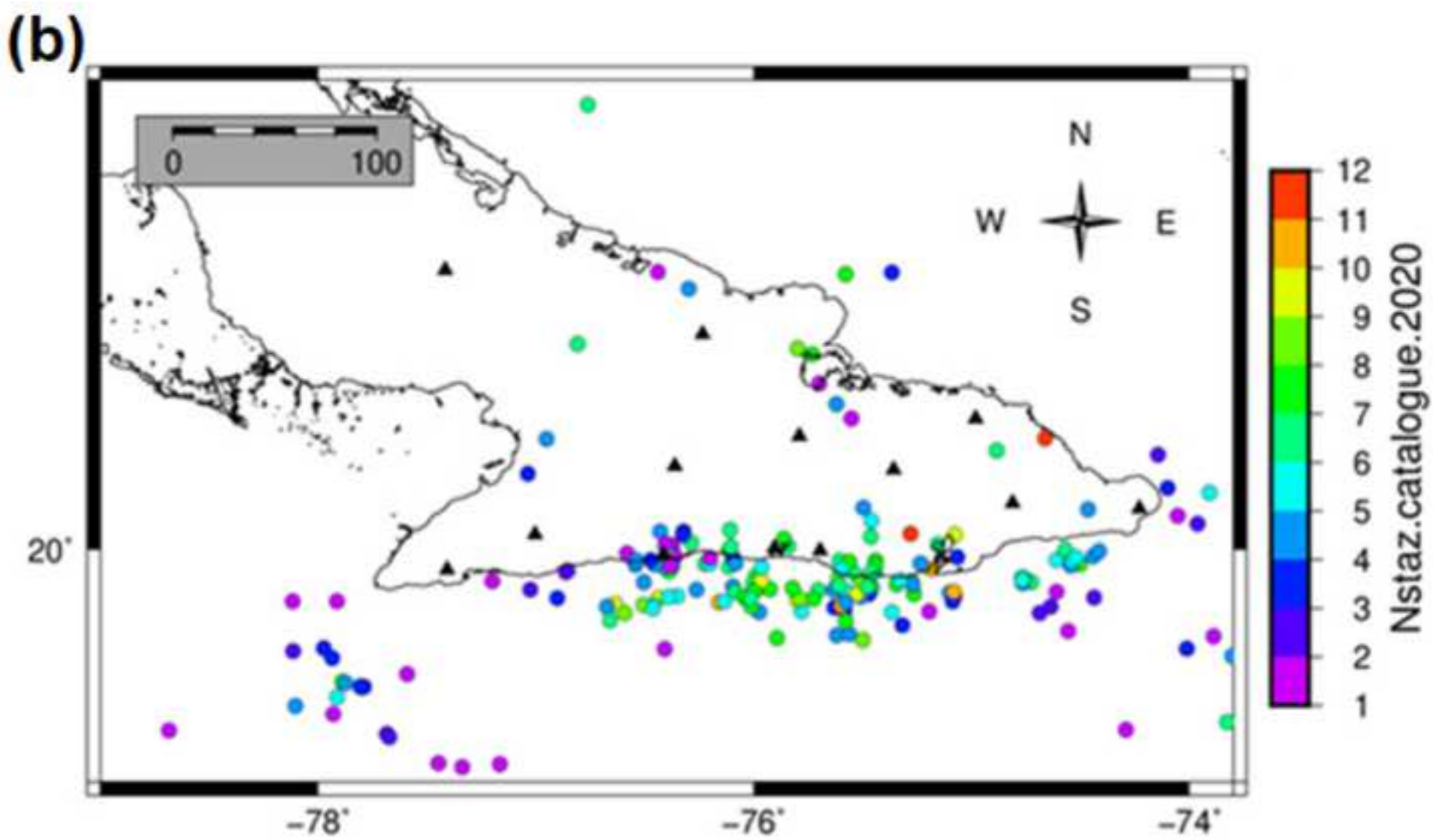

Electronic Supplemental Material
to
Evaluation of the detection level of the Cuban seismic network

by Eduardo R. Diez Zaldivar, Enrico Priolo, Denis Sandron, Viana Poveda Brossard, Marco Cattaneo, Simone Marzorati, Raúl Palau Clares

Submitted to Seismological Research Letters on January 12, 2022

Data Set DS01

The file named **collect_completo_2020.out** contains the Cuban 2020 earthquake catalog in SEISAN text format. It has been specifically compiled for this study. More details about the catalog format can be found in the SEISAN manual at https://www.uib.no/en/rg/geophysics/54592/software#seisan

Figure S1

Probability Density Functions (PDF) calculated using PQLX software from continuous recordings of seismic noise for all stations of the Cuban seismic network. Lines represent the following quantities: gray lines, the high- and low-reference noise models (Peterson models); continuous black line, the statistical parameter "Mode"; dashed black line, the statistical parameter "Mean"; white lines, statistical parameters "10%" (dashed line), "90%" (dashed line), and "95%" (solid line). (a) "Caibarién" station (CAIB). (b) "Camarioca" station (CAMR). (c) "Cascorro" station (CCCC). (d) "Chivirico" station (CHIV). (e) "Jaguey Grande" station (CJAG). (f) "Holguín" station (HLG). (g) "Las Mercedes" station (LMGC). (h) "Mar Verde" station (MARV). (i) "Maisí" station (MASC). (j) "Manicaragua" station (MGV). (k) "Nuevo Mundo" station (NMDO). (l) "Pilón" station (PILO). (m) "Quimbuelo" station (QMBU). (n) "Rio Carpintero" station (RCC). (o) ¨Soroa" station (SOR). (p) "Yarey" station (YAR). (q) "Sabaneta" station (SAB). (r) "Pinares de Mayari" station (PIN).

Figure S2

Estimated detection levels of the Cuban seismic network in terms of minimum detected magnitude for several combinations of the SNR value, number of triggered stations (NTS), and statistical variables "10%", "Mean", "Mode", and "95%", respectively. Rows: maps obtained for (top) SNR=2 and NTS=2 (ideal case but little used), (middle) SNR=2 and NTS=3, and (bottom) SNR=3 and NTS=4. Columns: maps obtained by varying statistical variables as indicated at the top of each column. The color represent the minimum detected magnitude. The red triangles show the location of the seismic stations.

Figure S3

Estimated detection levels of the Cuban seismic network in terms of number of triggered stations for an M_L1.0 earthquake hypothetically located at each point of the grid for several combinations of the SNR value, and statistical variables "10%", "Mean", "Mode", and "95%", respectively. Rows: maps obtained by varying the SNR over the values (top) SNR=2 (ideal case but little used), (middle) SNR =3, and (bottom) SNR=4. Columns: maps obtained by varying statistical variables as indicated at the top of each column. The color represent the number of triggered stations. The red triangles show the location of the seismic stations.

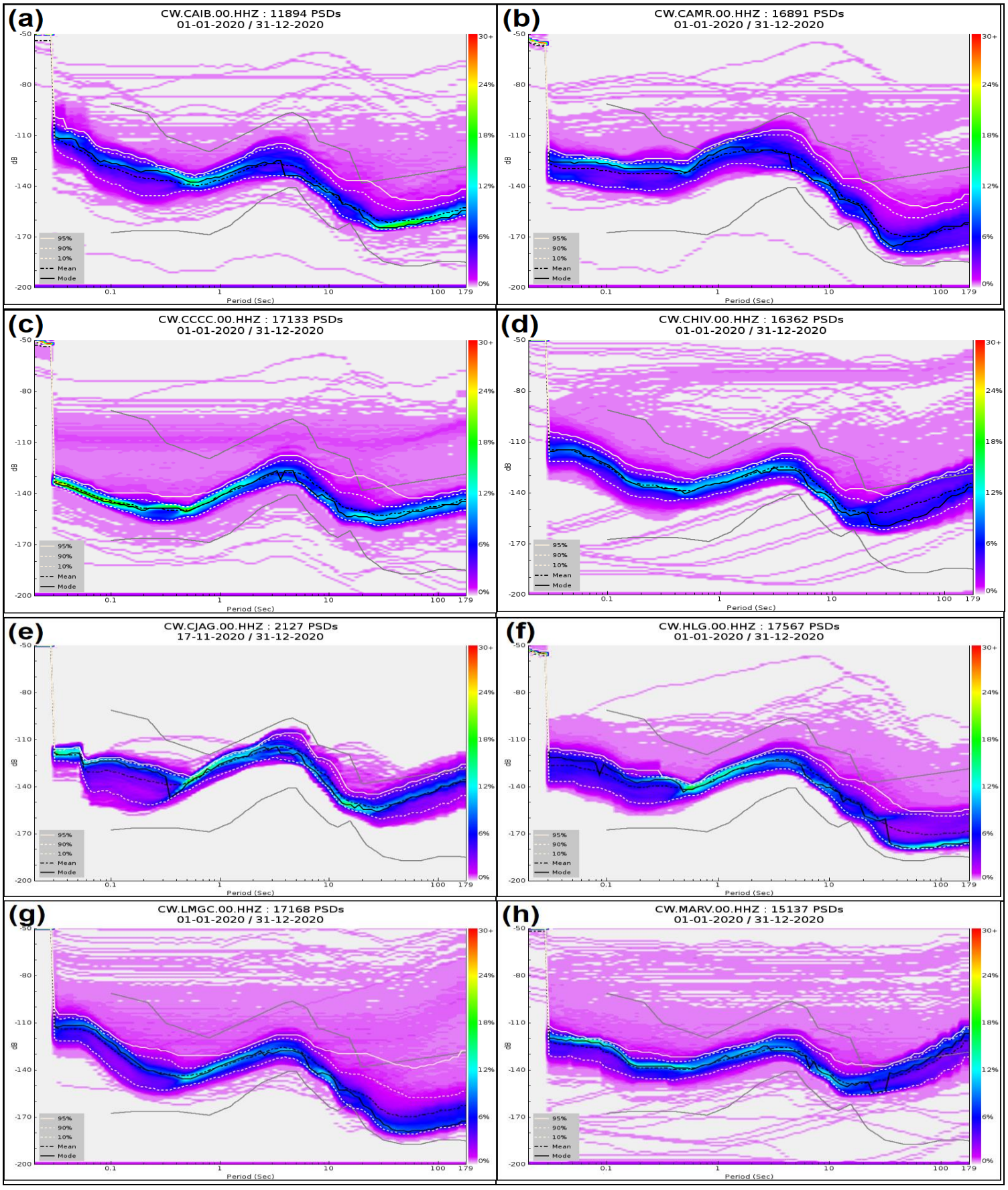
(a)
CW.CAIB.00.HHZ : 11894 PSDs
01-01-2020 / 31-12-2020
(b)
CW.CAMR.00.HHZ : 16891 PSDs
01-01-2020 / 31-12-2020
(c)
CW.CCCC.00.HHZ : 17133 PSDs
01-01-2020 / 31-12-2020
(d)
CW.CHIV.00.HHZ : 16362 PSDs
01-01-2020 / 31-12-2020
(e)
CW.CJAG.00.HHZ : 2127 PSDs
17-11-2020 / 31-12-2020
(f)
CW.HLG.00.HHZ : 17567 PSDs
01-01-2020 / 31-12-2020
(g)
CW.LMGC.00.HHZ : 17168 PSDs
01-01-2020 / 31-12-2020
(h)
CW.MARV.00.HHZ : 15137 PSDs
01-01-2020 / 31-12-2020
dB
Period (Sec)
95%
90%
10%
Mean
Mode

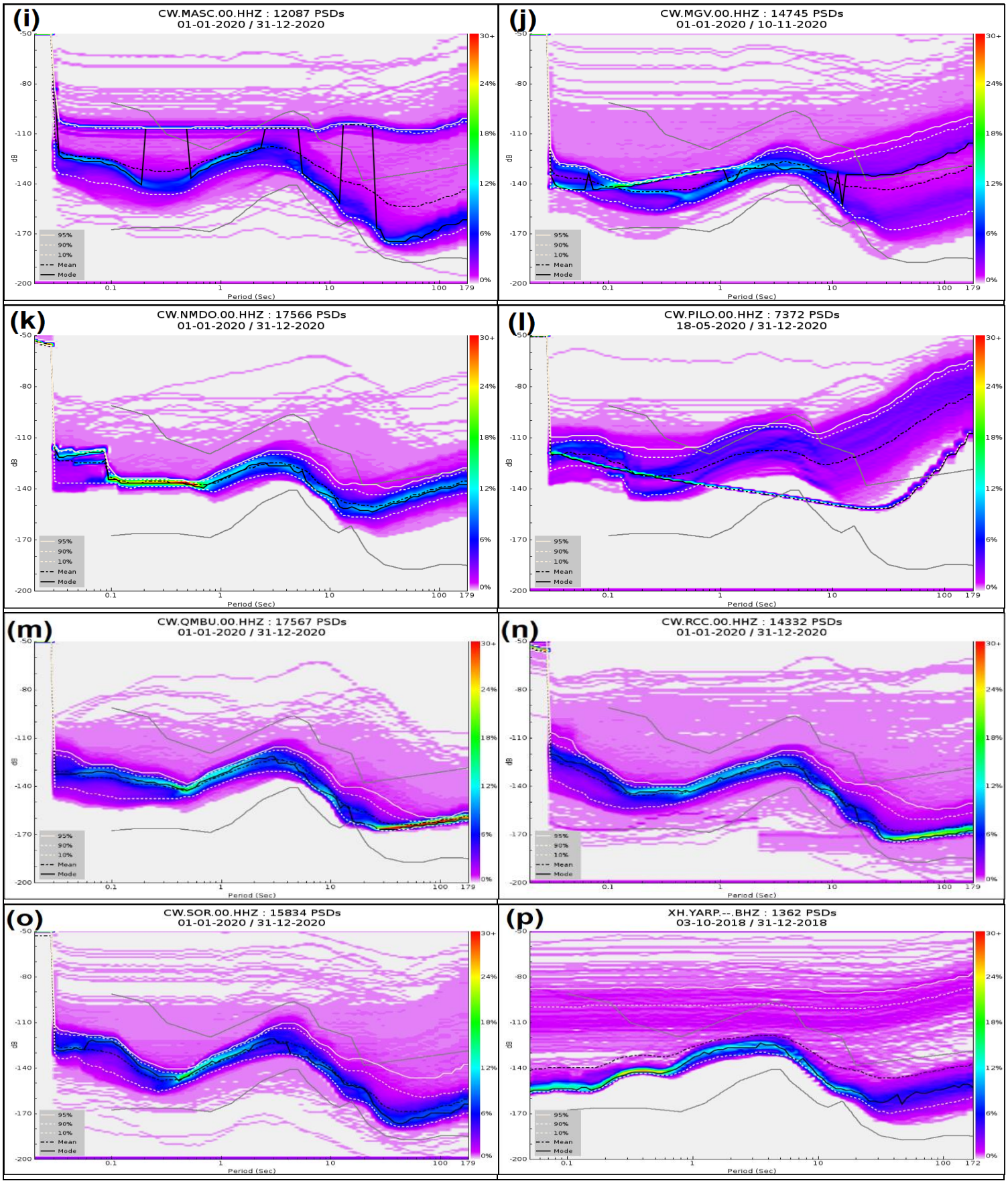
(i)
CW.MASC.00.HHZ : 12087 PSDs
01-01-2020 / 31-12-2020
(j)
CW.MGV.00.HHZ : 14745 PSDs
01-01-2020 / 10-11-2020
(k)
CW.NMDO.00.HHZ : 17566 PSDs
01-01-2020 / 31-12-2020
(l)
CW.PILO.00.HHZ : 7372 PSDs
18-05-2020 / 31-12-2020
(m)
CW.QMBU.00.HHZ : 17567 PSDs
01-01-2020 / 31-12-2020
(n)
CW.RCC.00.HHZ : 14332 PSDs
01-01-2020 / 31-12-2020
(o)
CW.SOR.00.HHZ : 15834 PSDs
01-01-2020 / 31-12-2020
(p)
XH.YARP.--.BHZ : 1362 PSDs
03-10-2018 / 31-12-2018
dB
Period (Sec)
95%
90%
10%
Mean
Mode

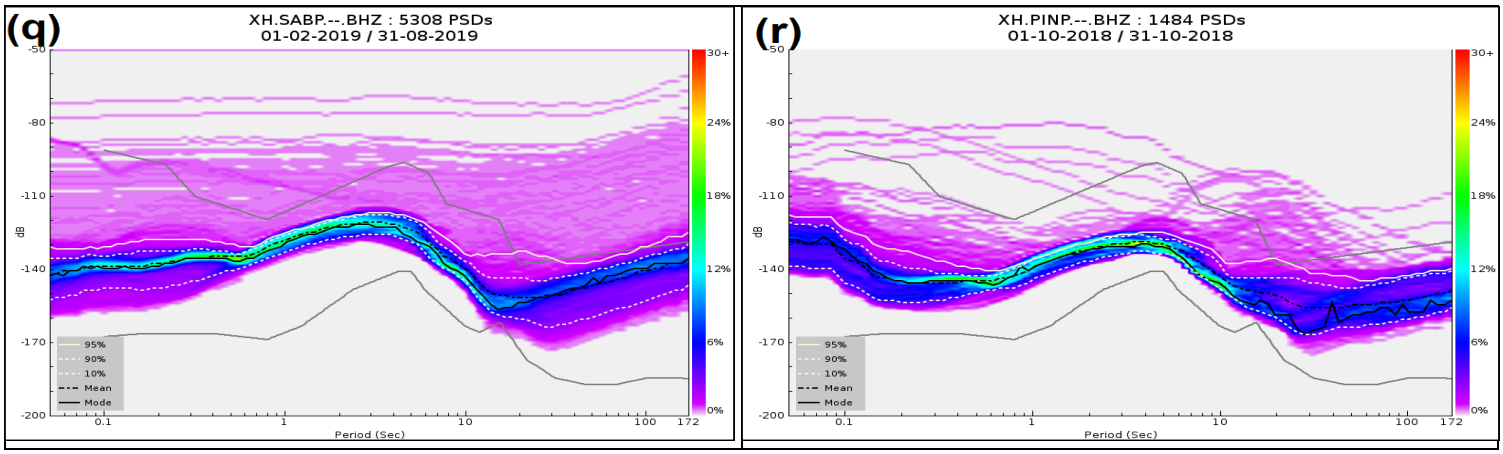
(q)
XH.SABP.--.BHZ : 5308 PSDs
01-02-2019 / 31-08-2019
(r)
XH.PINP.--.BHZ : 1484 PSDs
01-10-2018 / 31-10-2018
dB
Period (Sec)
95%
90%
10%
Mean
Mode
30+
24%
18%
12%
6%
0%

Figure S1

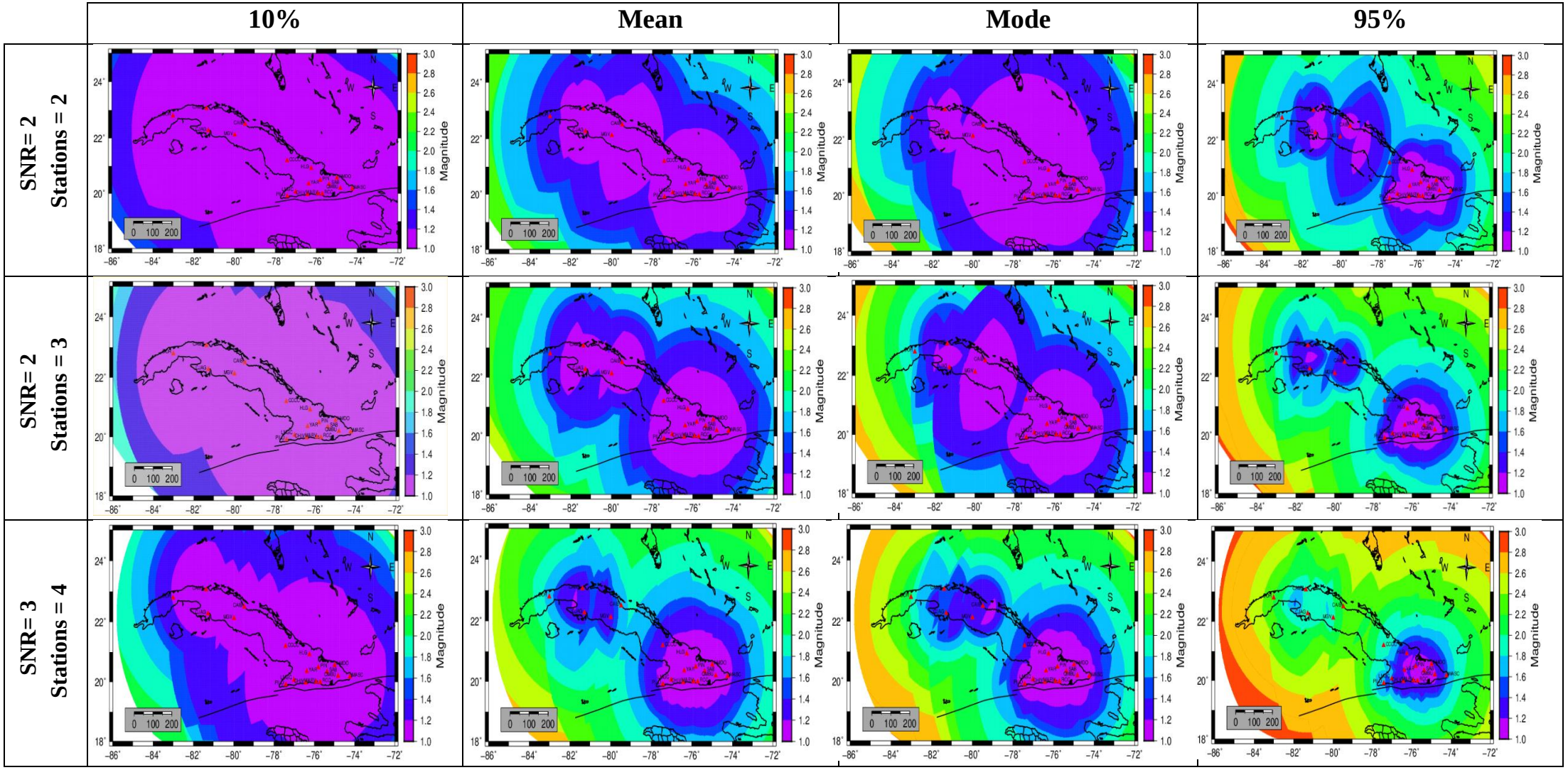
10%
Mean
Mode
95%
SNR= 2
Stations = 2
SNR= 2
Stations = 3
SNR= 3
Stations = 4
Magnitude
0 100 200

Figure S2

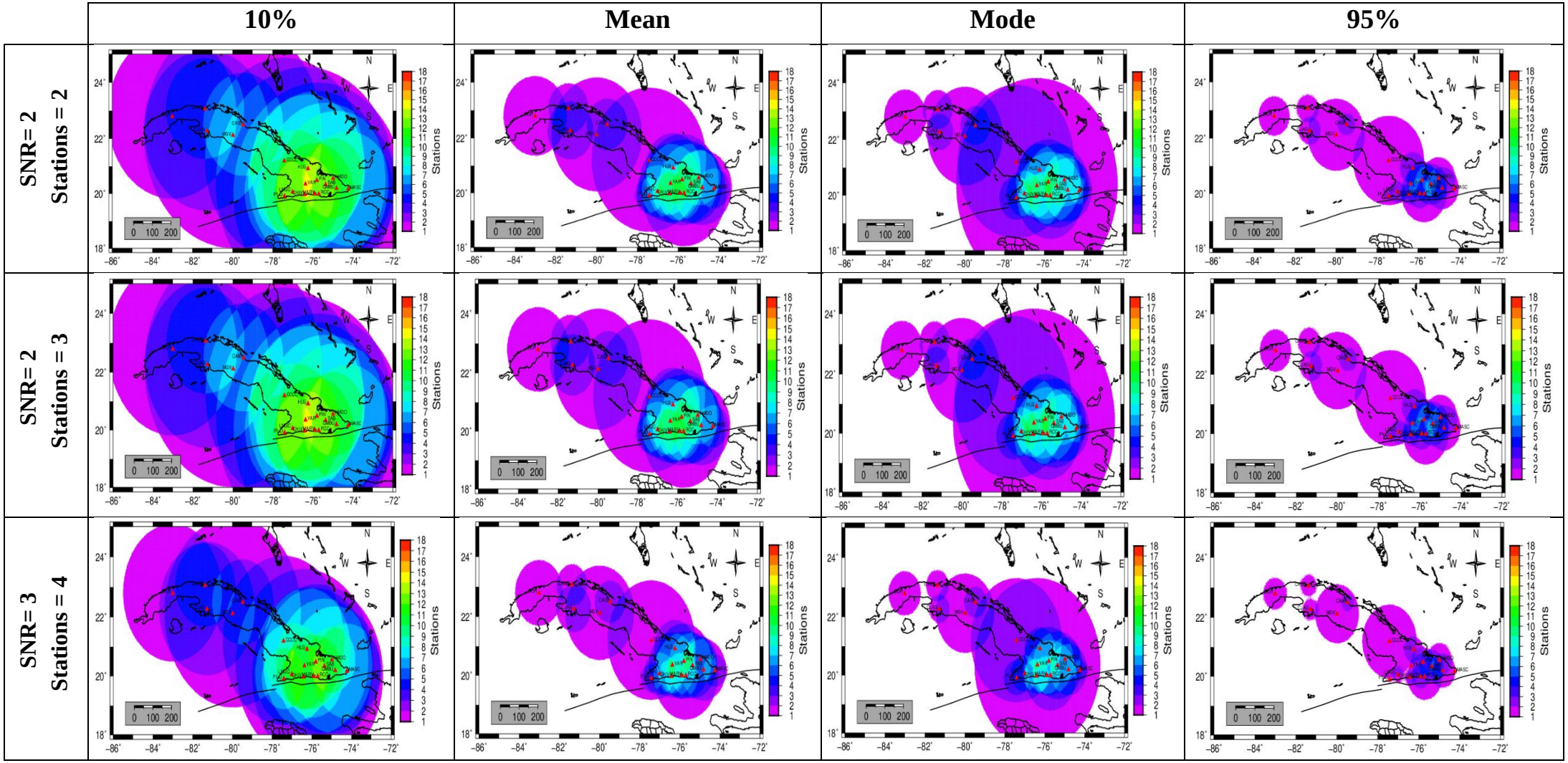
10%
Mean
Mode
95%
SNR= 2
Stations = 2
SNR= 2
Stations = 3
SNR= 3
Stations = 4
Stations
0 100 200

Figure S3

Click here to access/download

Supplemental Material (All Other Files, i.e. Movie, Zip, csv)

collect_completo_2020.out.zip